



Significance of the concentration gradients associated with dunite bodies in the Josephine and Trinity ophiolites

Zachary Morgan and Yan Liang

*Department of Geological Sciences, Brown University, Providence, Rhode Island 02912, USA
(yan_liang@brown.edu)*

Peter Kelemen

Lamont-Doherty Earth Observatory, Columbia University, Palisades, New York 10964, USA

[1] Detailed transects were sampled across dunite bodies in the Josephine and Trinity ophiolites. The major peridotite lithologies sampled in the Josephine transect are a sequence of dunite and harzburgite and in the Trinity transect a sequence of dunite, harzburgite, lherzolite, and plagioclase lherzolite (DHL-PL). Major, minor, and selected trace element abundances in olivine, orthopyroxene, clinopyroxene, and spinel were measured. The composition profile from the Josephine transect has revealed a concentration gradient near the dunite-harzburgite contact. The composition profile from the Trinity transect has revealed several concentration gradients: two within the dunite, one in the harzburgite, and at least two in the plagioclase lherzolite. The composition profiles record complex histories of melt transport, melt-rock reaction, and subsequent subsolidus reequilibration. Analyses of closure distance suggest that compositional variation trends for a majority of major and minor elements in olivine, clinopyroxene, orthopyroxene, and spinel reported in this study were magmatic in origin. Subsolidus reequilibration may reduce the range or magnitude of variations for the 2+ cations such as Fe and Mg in olivine and spinel and significantly redistribute Ca and Li in coexisting minerals. Numerical simulations exploring the coupling of diffusion and advection in a porous matrix were used to explain compositional variations across the peridotite sequences. Melt flow from the host harzburgite into the dunite produces composition gradients near the dunite-harzburgite contacts similar to those from the Josephine transect. In contrast, melt flow from the dunite into the surrounding peridotite lithologies can produce concentration gradients similar to those observed in the Trinity transect. At least two chemically distinct episodes of melt flow within the same dunite channel system are proposed. Results from this study show that concentration gradients developed around the dunite-harzburgite and DHL-PL sequences can be used to infer part of the melt flow history of the dunite channel systems in the mantle. Results from this study and those from other ophiolite studies also demonstrate that concentration profiles in dunite and the surrounding peridotite lithologies are highly variable even among differing peridotite sequences within the same ophiolite, suggesting that the composition of instantaneous melt flowing through individual dunite channels is quite variable and the mantle source regions are heterogeneous.

Components: 14,711 words, 20 figures.

Keywords: dunite; harzburgite; lherzolite; melt-rock reaction; reactive dissolution; concentration gradient.

Index Terms: 8412 Volcanology: Reactions and phase equilibria (1012, 3612); 8416 Volcanology: Mid-oceanic ridge processes (1032, 3614); 8434 Volcanology: Magma migration and fragmentation.



Received 22 January 2008; Revised 4 June 2008; Accepted 6 June 2008; Published 29 July 2008.

Morgan, Z., Y. Liang, and P. Kelemen (2008), Significance of the concentration gradients associated with dunite bodies in the Josephine and Trinity ophiolites, *Geochem. Geophys. Geosyst.*, 9, Q07025, doi:10.1029/2008GC001954.

1. Introduction

[2] Dunites are commonly observed in the mantle sections of ophiolite and peridotite massifs around the world [e.g., *Boudier and Nicolas*, 1985]. They occur as veins, and tabular or sometimes irregular shaped bodies in the host harzburgite or plagioclase-bearing lherzolite and are interpreted as remnants of conduits or channels for melt migration in the mantle [e.g., *Kelemen et al.*, 1997, and references therein]. On the basis of dominant lithology, *Boudier and Nicolas* [1985] divided ophiolites into harzburgite subtype and lherzolite subtype. Dunite in lherzolite subtype ophiolite is surrounded by a layer of harzburgite that, in turn, is surrounded by a layer of plagioclase-free lherzolite, and finally the plagioclase-bearing lherzolite, forming the dunite, harzburgite, lherzolite, and plagioclase lherzolite (DHL-PL) sequence (Figure 1a). Dunite in harzburgite subtype ophiolite is simply surrounded by harzburgite (Figure 1b).

[3] The distinct peridotite sequences have also been observed in high-temperature and high-pressure reactive dissolution experiments involving melt-bearing peridotite and basalt [*Daines and Kohlstedt*, 1994; *Morgan and Liang*, 2003, 2005; *Beck et al.*, 2006]. Depending on starting peridotite mineralogy, these dissolution experiments produce either a melt-bearing dunite-harzburgite or dunite-harzburgite-lherzolite sequence. The melt-bearing dunites produced in these experiments are orthopyroxene-free, while the melt-bearing harzburgites produced in the lherzolite dissolution experiments are clinopyroxene-free. Another interesting feature of the harzburgite or lherzolite dissolution experiments is the presence of simple concentration gradients in minerals across the peridotite sequences. Figure 2 is a summary of recent experimental observations illustrating the lithological and chemical variations. The broad compositional variations across dunite-harzburgite contact and harzburgite-lherzolite contact result from a combined effect of orthopyroxene (opx) dissolution at the dunite-harzburgite interface, clinopyroxene (cpx) dissolution at the harzburgite-lherzolite interface, olivine precipitation within the dunite, and diffusive exchange between the crystals and the melts in the

dunite, harzburgite, and lherzolite [*Liang*, 2003; *Morgan and Liang*, 2003, 2005]. The growth of the dunite layer in these diffusive dissolution experiments is controlled by the rates of diffusion of major elements in the melt and the extent of undersaturation of opx with respect to the dissolving magma.

[4] In the presence of grain-scale melt flow, which is likely for melt migration in at least part of the upper mantle, there exists a positive feedback between flow and dissolution as olivine normative basalt generated at greater depth percolating through a porous harzburgite or lherzolite matrix [e.g., *Daines and Kohlstedt*, 1994; *Aharonov et al.*, 1995; *Kelemen et al.*, 1995b, 1997; *Spiegelman et al.*, 2001]. The extent of melt-peridotite interaction also depends on the rates and directions of melt flow with respect to lithological contact. As in peridotite dissolution experiments, records of melt-peridotite interaction can be preserved or partly preserved in the dunite-harzburgite or DHL-PL sequence. Indeed, mineral compositional variations across dunite-harzburgite or DHL-PL sequences from ophiolites or peridotite massifs have been reported in a number of studies [e.g., *Quick*, 1981a; *Obata and Nagahara*, 1987; *Kelemen et al.*, 1992; *Takahashi*, 1992; *Takazawa et al.*, 2000; *Kubo*, 2002; *Suhr et al.*, 2003; *Braun*, 2004; *Lundstrom et al.*, 2005; *Zhou et al.*, 2005]. In general, mineral compositional variations observed in the field are more complicated than those observed in peridotite dissolution experiments, reflecting more complicated geological processes involved in the nature. Figure 1c illustrates some of the variability of NiO in olivine from the Bay of Islands ophiolite [*Suhr et al.*, 2003]. Three different types of NiO in olivine profiles were observed: the NiO content of olivine in the dunite is (1) lower than that in the surrounding harzburgite (Figure 1c, solid line), (2) greater than that in the host harzburgite (dotted line), and (3) approximately the same as that in the harzburgite (dashed line). Compositional trends similar to cases 2 and 3 were also observed for the Mg# in olivine from the Bay of Islands ophiolite [*Suhr et al.*, 2003]. Explanations for the observed compositional variations include different degrees of partial melting, and/or various extents of

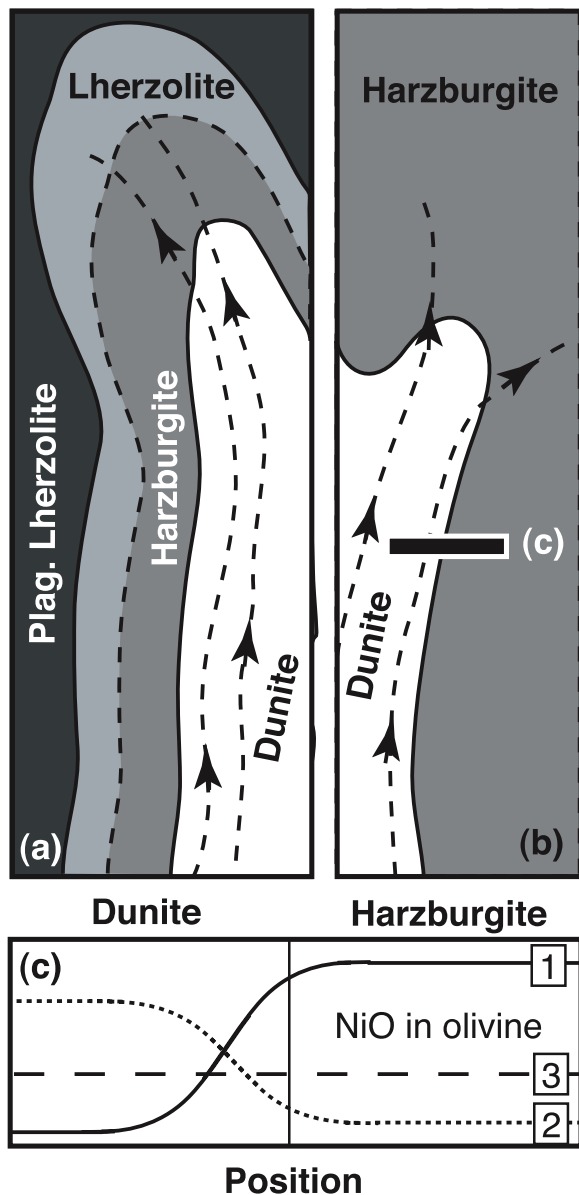


Figure 1. (a) A hypothetical dunite-harzburgite-lherzolite-plagioclase lherzolite sequence with sharp lithological contacts. (b) Schematic representation of a dunite-harzburgite sequence with sharp lithological contacts. (c) Schematic composition profiles for NiO in olivine from the Bay of Islands ophiolite [after Suhr *et al.*, 2003]. The solid lines are based on dunite traverses BMD-A, BMD-C, and NA30 with dunite widths ranging from 4 to 10 m. The dashed line is based on dunite traverses T1172 and T1581 with dunite widths ranging from 0.15 to 15 m. The dotted line is for dunite traverse T1537 with a dunite width of 15 m [Suhr *et al.*, 2003].

melt-rock reaction. Another interesting feature associated with compositional variations across a dunite-harzburgite or DHL-PL sequence is the spatial range over which mineral and bulk rock composition vary with respect to the nearest lithological contact: the latter, in general, is not centered at the former. In the case of NiO abundance in olivine shown in Figure 1c, spatial locations of the main compositional variations are shifted to the dunite side of the dunite-harzburgite interface. As will be shown in this study, the shift in concentration gradient is likely resulted from melt flow across lithological boundaries.

[5] Motivated by our harzburgite and lherzolite dissolution experiments, we systematically sampled a number of dunite-harzburgite sequences at the Josephine ophiolite (in southern Oregon) and

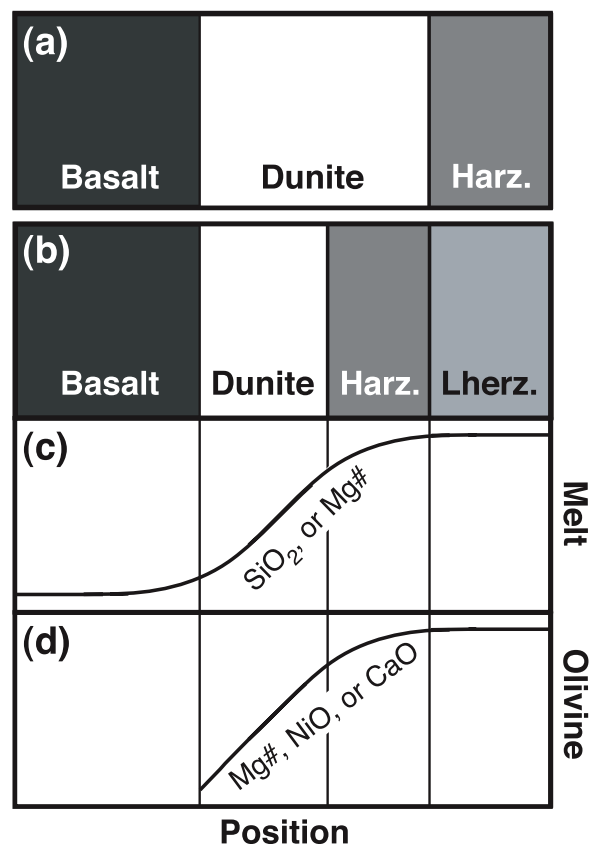


Figure 2. (a) Schematic representation of an experimentally produced dunite-harzburgite sequence from Morgan and Liang [2003]. (b) Schematic representation of an experimentally produced dunite-harzburgite-lherzolite-plagioclase lherzolite (DHL-PL) sequence from Morgan and Liang [2005]. (c) Schematic composition profile for SiO₂ or Mg# in the melt as a function of position. (d) Mg#, NiO, or CaO in olivine within the experimentally produced peridotite sequence [Morgan and Liang, 2005].



DHL-PL sequences at the Trinity ophiolite (in northern California). In this report, we present a detailed compositional traverse across a dunite (3.64 m wide), harzburgite-lherzolite (5.64 m), and plagioclase lherzolite (>10 m) sequence at the Trinity ophiolite and a detailed compositional traverse across a dunite (13 m wide) and harzburgite sequence at the Josephine ophiolite. No compositional traverses have been reported for the Josephine ophiolite. Data on major element variations across DHL-PL sequences in the Trinity ophiolite are limited. On the basis of electron microprobe analyses of coexisting minerals in 5 samples, *Quick* [1981a] showed the existence of broad compositional trends across a 0.2 m wide dunite and associated peridotites (0.7 m wide) in the Trinity ophiolite. Our high-resolution compositional traverse for a DHP-PL sequence from the Trinity ophiolite also compliments to the trace element studies of *Kelemen et al.* [1992] and *Lundstrom et al.* [2005], who reported REE, Li, and B abundance in cpx across several DHL-PL sequences in the Trinity ophiolite. In section 4 we first compare our measured concentration profiles with those from other ophiolites and peridotite massifs, and then discuss the effect of subsolidus reequilibration on the observed mineral compositional variations. We will show that subsolidus reequilibration redistributes at least some of the fast diffusing cations, such as Ca and Li, in peridotite minerals. For elements that are not significantly affected by subsolidus reequilibration processes, we explore the significance of their spatial variations across dunite-harzburgite or DHL-PL sequences in section 7. With the help of a simple numerical model, we will show that, in addition to dissolution and diffusive exchange, melt flow across lithological contacts likely play an important role in producing the observed concentration patterns in minerals across various lithological units.

2. Field Descriptions

[6] This study focuses on two dunite bodies and the host peridotite from the Josephine and Trinity ophiolites. Following the nomenclature of *Boudier and Nicolas* [1985], the Josephine ophiolite is a harzburgite subtype ophiolite and the Trinity ophiolite is a lherzolite subtype ophiolite.

2.1. Josephine Ophiolite

[7] The Josephine ophiolite is found in the Klamath Mountains of southwest Oregon and northern California [*Himmelberg and Loney*, 1973; *Loney and Himmelberg*, 1976; *Dick*, 1977a, 1977b; *Harper*,

1980, 1984; *Kelemen and Dick*, 1995] and is dated at 157 Ma (U/Pb age of zircon [*Saleeby et al.*, 1982]). The mantle section of the Josephine ophiolite is dominated by harzburgite containing pyroxene rich bands and minor amounts of dunite [*Dick*, 1977b]. The harzburgite is dominated by olivine and opx with minor amounts of cpx and spinel.

[8] This work focuses on the Fresno Bench region of the Josephine ophiolite, which has been previously described by *Kelemen and Dick* [1995]. Structurally, the Fresno Bench region shows evidence for both high-temperature melt migration and high-temperature deformation. Numerous high-temperature, mylonitic shear zones defined by deformation of the ubiquitous pyroxene enriched bands within the harzburgite, sharp decrease in olivine, spinel, and opx grain size and the alignment of individual opx and spinel crystals are observed [*Kelemen and Dick*, 1995]. The relationship between melt migration and deformation is complicated, with evidence for melt migration both prior to (i.e., deformation of a small dunite body) and during deformation (i.e., anastomosing dunite within shear zones; see *Kelemen and Dick* [1995] for a detailed discussion).

[9] Our sampling traverse focused on the largest dunite-harzburgite sequence in the Fresno Bench region of the Josephine ophiolite [*Kelemen and Dick*, 1995]. The sequence is as follows. To the south of the dunite is massive harzburgite containing periodic pyroxene rich bands. The contact between the dunite and the harzburgite is sharp but irregular as shown in Figure 3. The main body of the dunite is approximately 13 m wide with a small pyroxene bearing lens within the dunite about 0.25 m from the contact. The north side of the dunite transitions to roughly 15 m of interlayered dunite and harzburgite before returning to massive harzburgite. We collected samples along a transect perpendicular to the dunite-harzburgite contact. Within approximately 1 m on either side of the dunite-harzburgite contact we sampled continuously, further away we collected one sample roughly every meter. Brief descriptions of the sampled lithologies are presented in auxiliary material Text S1.¹

2.2. Trinity Ophiolite

[10] The Trinity ophiolite is located in the eastern Klamath Mountains of northern California [*Quick*,

¹Auxiliary material data sets are available at <ftp://ftp.agu.org/apend/gc/2008gc001954>. Other auxiliary materials are in the HTML.

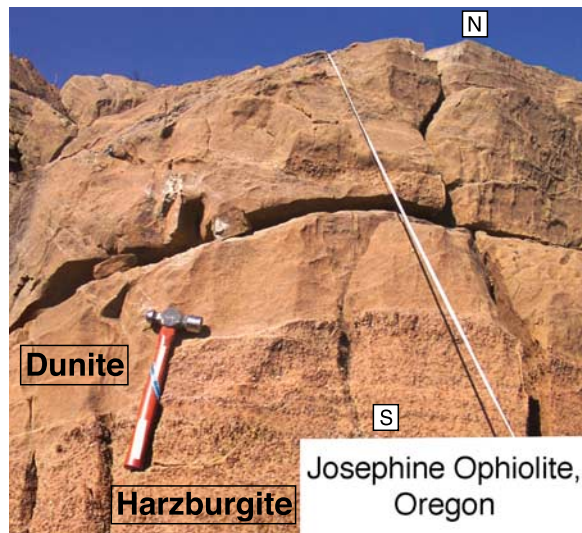


Figure 3. Photograph of the outcrop sampled at the Josephine ophiolite. This photo illustrates the dunite-harzburgite contact. The dunite is the smooth material on the upper two thirds of the image, and the harzburgite is the rough material on the bottom edge. North (N) and south (S) are marked.

1981b; Carter and Quick, 1987; Kelemen *et al.*, 1992]. The age of the ophiolite is between 402 Ma and 472 Ma (whole rock Sm-Nd, 402 Ma to 472 Ma [Jacobsen *et al.*, 1984; Gruau *et al.*, 1995] and U/Pb age of zircon 404 Ma to 431 Ma [Wallin and Metcalf, 1998]). The main ultramafic

lithologies at the Trinity ophiolite include plagioclase lherzolite, lherzolite, harzburgite, dunite, clinopyroxenite and websterite [Quick, 1981b; Carter and Quick, 1987].

[11] This work focused on a large DHL-PL sequence in the Eunice bluff region of the Trinity ophiolite [Quick, 1981a; Carter and Quick, 1987]. This peridotite sequence was initially sampled by Kelemen *et al.* [1992] (transect TP90-20) [see also Lundstrom *et al.*, 2005]. The sequence is as follows. To the east of the dunite is Quaternary glacial till. Continuing westward the dunite is roughly 3 m wide. The contact between the dunite and the harzburgite is sharp but irregular as shown in Figure 4. The dunite contains a small clinopyroxenite vein, approximately 10 mm wide, centered 0.86 m from the dunite-harzburgite contact. The harzburgite/lherzolite sequence is roughly 5.5 m wide. The exact position of the contact between the harzburgite and lherzolite was difficult to see in the field. However, our preliminary modal abundance data suggests the contact may occur approximately 2.5 m from the dunite-harzburgite contact (see section 4.2). Continuing further west the contact between the lherzolite and the plagioclase lherzolite is again sharp but irregular. The plagioclase lherzolite continues through the end of the outcrop. We collected samples along a transect perpendicular to the dunite-harzburgite contact. Within 1 m on

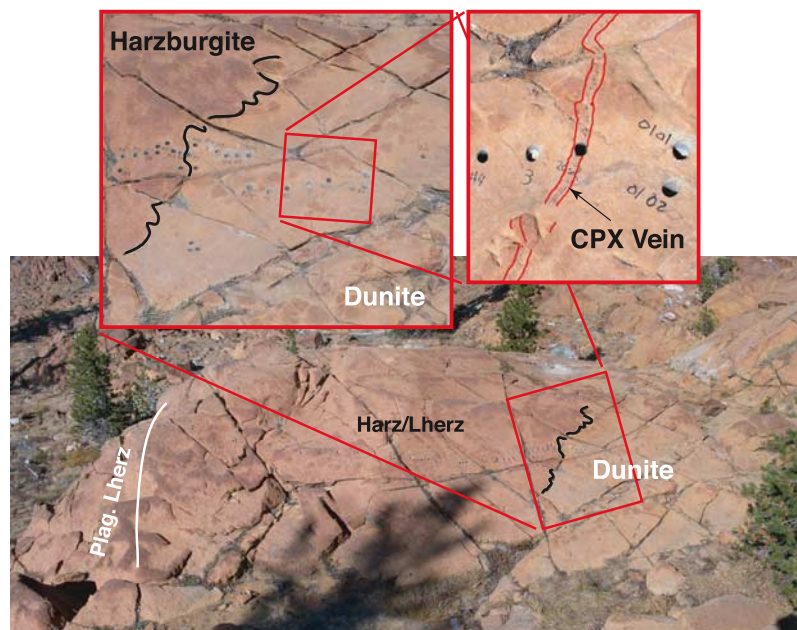


Figure 4. Photograph of the outcrop sampled at the Trinity ophiolite. Large image on the bottom illustrates most of the dunite-harzburgite-lherzolite-plagioclase lherzolite sequence. The black line is the trace of the dunite-harzburgite contact. The pyroxenite vein is outlined in red.



either side of the dunite-harzburgite contact we sampled every 0.05 to 0.06 m, further away we collected one sample approximately every 0.25 m through the harzburgite-lherzolite region. A brief description of the sampled lithologies is presented in the auxiliary material Text S1.

3. Chemical Analysis

3.1. Electron Microprobe

[12] Major, minor, and selected trace elements in olivine, opx, cpx, and spinel were analyzed using a Cameca SX100 electron microprobe at Brown University. An accelerating voltage of 20 kV and a focused beam with beam current of 25 nA was used for all mineral analyses. Counting times of 30 and 15 s were used for peak and background position, respectively. Natural mineral standards were used and the ZAF correction was employed.

[13] We treat each sample (a thin section or a 25.4 mm diameter drill core mount) from the two ophiolites as a spatially distinct sample. For each mineral we measure approximately 10 points from around the thin section. The points were chosen as close as possible to the core of a grain in order to minimize the effects of zonation, alteration, and reequilibration. These 10 points are then averaged to produce a mean composition for a given sample. However, zoning of Al₂O₃, TiO₂ and the REE was observed in cpx and opx from the Trinity ophiolite [Quick, 1981b; M. Lo Cascio, personal communication, 2005] and may result in larger scatter in the pyroxene compositions. Results of the mineral analyses are reported in Figures 6–9 and Tables S1c–S1f in auxiliary material Table S1 for the Josephine ophiolite samples and Figures 11–14 and Tables S2c–S2f in auxiliary material Table S2 for the Trinity peridotite samples.

3.2. Ion Microprobe

[14] Despite the low overall abundance of cpx within each dunite sample we measured rare earth element (REE) compositions from cpx within 4 Trinity dunite samples using a Cameca IMS 3f ion probe at Woods Hole Oceanographic Institution. An O²⁻ primary beam with a current of 35–40 nA and beam spot of 20–30 μm were used in the analysis. The secondary ions were filtered with a –60 to –90 V energy window [Shimizu and Hart, 1982]. Owing to the limited size and abundance of cpx we only made 2 or 3 REE measurements of cpx in each of the 4 dunite samples (Figure 15 and Table S2g in auxiliary material Table S2).

3.3. Bulk Chemical Analyses

[15] The coarse grain size of the peridotite lithologies in the Josephine and Trinity ophiolites and the small sample size of our Trinity samples limit our ability to measure the modal abundances of our peridotite samples. As an attempt to estimate the modal abundances, a number of samples from both ophiolites were selected for bulk chemical analysis. To minimize contamination, the selected Josephine ophiolite samples were crushed between two blocks of Plexiglas using a hydraulic press. The Trinity samples were crushed in a Tungsten-Carbide mill. A selection of Josephine ophiolite samples were sent to the Washington State University GeoAnalytical lab for XRF and ICP-MS analysis and the remainder of the samples were sent to Franklin and Marshall College for XRF analysis. The XRF analyses of the Trinity ophiolite samples were conducted at Franklin and Marshall College. Bulk chemical analyses are reported in Tables S1a and S2a in auxiliary material Tables S1 and S2, respectively.

4. Results

[16] At both the Josephine and Trinity ophiolites, we measured the mineral and bulk rock compositions as a function of position across a dunite dike and the associated peridotite sequence. For clarity we organize the chemical results first by ophiolite and then by the mineral analyzed and discuss the composition profiles in a particular mineral across the peridotite sequence.

4.1. Josephine

[17] The modal abundances for several samples within the dunite and the harzburgite were calculated using a linear least squares inversion of the bulk and mineral chemistry data for these samples. These data should be viewed as semiquantitative because of the altered nature of the samples (auxiliary material Text S1). Figure 5 displays the calculated modal abundances of our Josephine samples. The dunite is primarily olivine (>90 wt%) with at most 2% spinel (see also Table S1b in auxiliary material Table S1). The low total modal abundance (olivine + spinel) calculated for the dunite is the result of pervasive alteration to serpentine and magnetite in the dunite and serpentine, tremolite, talc and magnetite in the harzburgite. The harzburgite is primarily olivine with 10 to 15% opx and 2% cpx and spinel. Aside from chromitite bands (unsampled) the spinel abundance is relatively

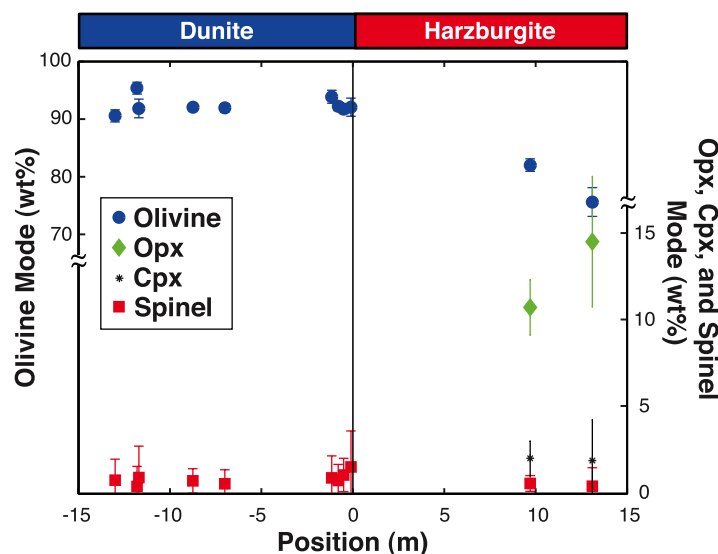


Figure 5. Modal abundance (wt%) of olivine (blue circles), opx (green diamonds), cpx (black asterisks), and spinel (red squares) in the Josephine ophiolite samples. The modal abundances were calculated from the bulk chemical data and individual mineral analyses and are listed in Table S1b of auxiliary material Table S1.

uniform throughout the dunite and the harzburgite (Figure 5).

4.1.1. Olivine

[18] Figure 6 displays the Mg#, MnO, NiO and CaO in olivine as a function of position across the dunite-harzburgite sequence. The Mg# and NiO in olivine increases from the harzburgite to the dunite. The MnO in olivine decreases from the harzburgite into the dunite. Finally, the CaO content of olivine within the dunite is higher than the surrounding harzburgite. Overall, these features are similar to measurements made across dunite-harzburgite sequences at other ophiolites (e.g., Bay of Islands ophiolite [Suhr *et al.*, 2003] and Oman ophiolite [Braun, 2004]).

4.1.2. Spinel

[19] Spinel compositions from the Josephine traverse show a similar composition profile to the one observed in olivine. Figure 7 displays the Mg#, Cr#, and TiO₂ in spinel as a function of position. The average Mg# in spinel decreases from the harzburgite to the dunite, whereas Cr# and TiO₂ in spinel increases from the harzburgite to the dunite.

4.1.3. Pyroxene

[20] Pyroxenes are limited to the harzburgite. Figures 8 and 9 display the Mg# and selected oxide abundances in opx and cpx, respectively, as

a function of position. The limited data suggests that the Mg# of both opx and cpx increase close to the dunite-harzburgite contact, consistent with the results for Mg# in olivine. The Na₂O content of the cpx increases abruptly at the position sampled furthest from the dunite-harzburgite (Figure 9).

4.1.4. Chemical Boundary Layers

[21] Figures 6–9 include dotted and a dashed lines marking our interpretations of the dunite and harzburgite chemical boundary layers, respectively. We define the chemical boundary layer as the distance from the lithologic contact to the chemically uniform region within dunite or harzburgite, respectively. It should be noted that these boundary layers are not necessarily uniform and may differ for each mineral and chemical species. Figures 6–9 show that our measured boundary layers are asymmetric. The dunite boundary layer is approximately 1.16 m thick, whereas the harzburgite boundary layer is about 0.39 m thick (Figures 6 and 7). The width of both boundary layers is consistent among most components in olivine and spinel. Similarly the opx and cpx analyses have suggested harzburgite boundary layer thicknesses consistent with those from olivine and spinel data. The significance of these chemical boundary layers will be discussed in section 6.

4.2. Trinity

[22] Figure 10 displays the calculated modal abundance of olivine, opx, cpx and spinel as a function of

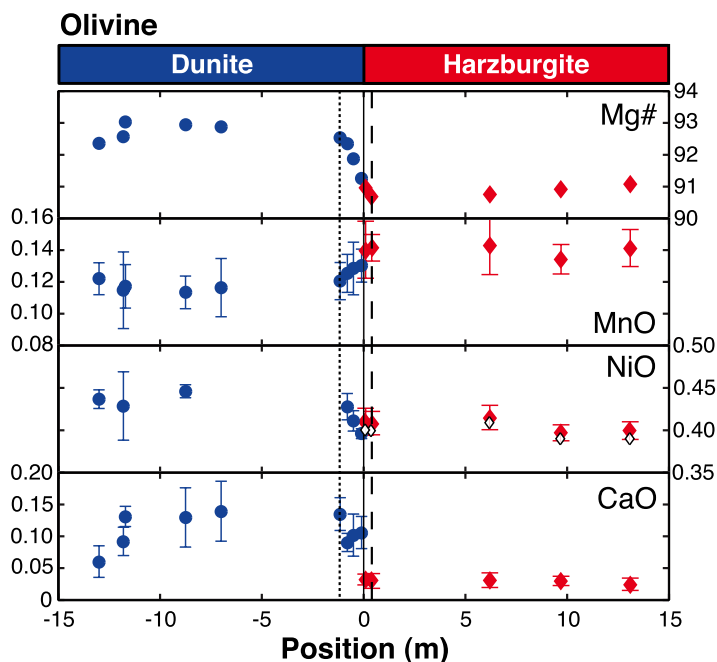


Figure 6. Composition profiles in olivine across the dunite-harzburgite sequence at the Josephine ophiolite. The blue circles and red diamonds are average of olivine analyses for each sample within the dunite and the harzburgite, respectively. The error bars are 1 standard deviation about the mean of all olivine analyses for a given sample. The distance from the dotted line to the dunite-harzburgite contact is the dunite boundary layer thickness. The distance from the dashed line to the dunite-harzburgite contact is the harzburgite boundary layer thickness. The open diamonds on the NiO panel are NiO compositions corrected for subsolidus equilibration.

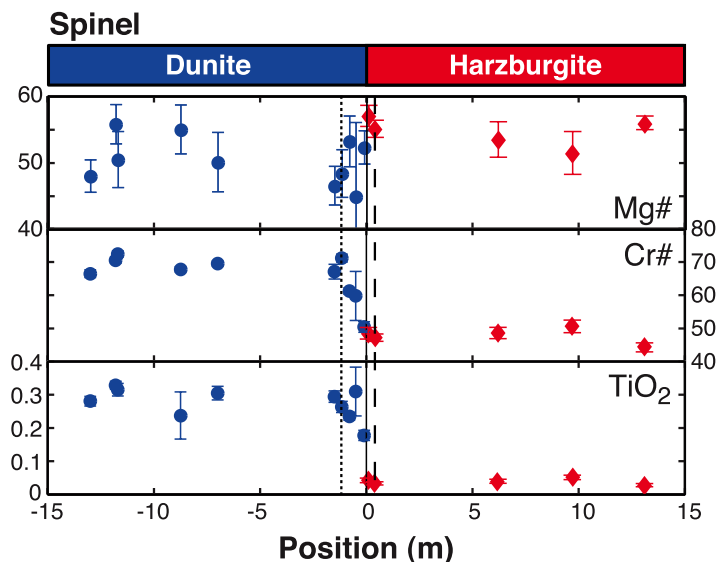


Figure 7. Composition profiles in spinel across the dunite-harzburgite sequence at the Josephine ophiolite. The blue circles and red diamonds are the average of spinel analyses for each sample within the dunite and the harzburgite, respectively. The error bars are 1 standard deviation about the mean of all spinel analyses for a particular sample. The distance from the dotted line to the dunite-harzburgite contact is the dunite boundary layer thickness. The distance from the dashed line to the dunite-harzburgite contact is the harzburgite boundary layer thickness.

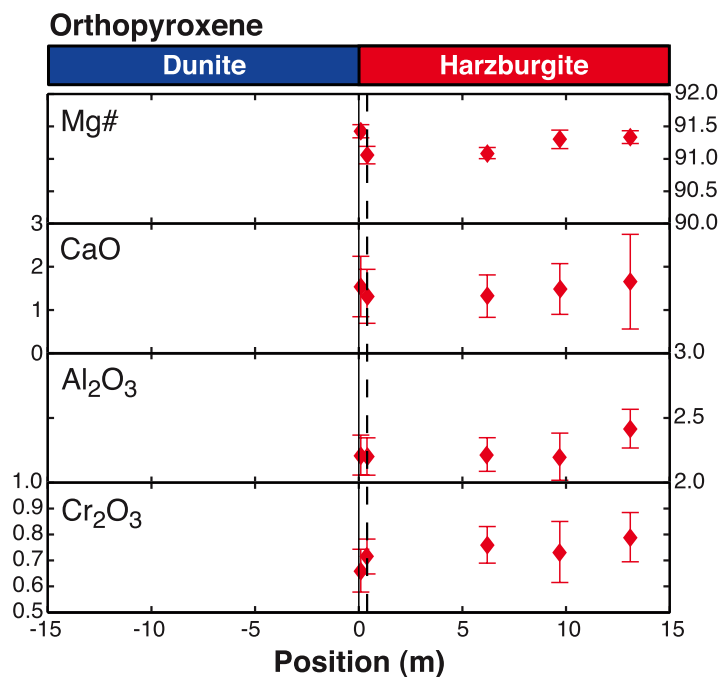


Figure 8. Composition profiles in orthopyroxene across the dunite-harzburgite sequence at the Josephine ophiolite. The red diamonds are the average of orthopyroxene analyses for each sample within the harzburgite. The error bars are 1 standard deviation about the mean of all orthopyroxene analyses for a particular sample. The distance from the dashed line to the dunite-harzburgite contact is the harzburgite boundary layer thickness.

position from our Trinity traverse (see also Table S2b in auxiliary material Table S2). Again these data should be read as semiquantitative because of the extensive alteration to serpentine, tremolite, talc and magnetite (auxiliary material Text S1). We have no modal abundance data for samples collected at positions greater than 4 m away from the dunite-harzburgite contact, because bulk chemical analyses were not available. The dunite is primarily olivine with less than a percent of cpx and spinel. Contained within the dunite is a small clinopyroxenite vein (5 to 10 mm wide, located at -0.86 m). The actual sample used for the bulk chemical analysis was collected next to the vein and does not show an apparent increase in model cpx. At the dunite-harzburgite contact the olivine mode decreases, and the opx and, to a lesser extent, the cpx mode increases. Within the harzburgite region the modal abundance of opx has a maximum of 27% at 1.08 m and decreases further into the harzburgite/lherzolite region (Figure 10). The cpx abundance increases to about 5% at 2.5 m or about halfway through the harzburgite/lherzolite region (Figure 10). This increase in cpx modal abundance may be the transition from the harzburgite to the lherzolite. However, our bulk analytical data is limited and only contains 3 points in the “lherzolite” region. The modal abundance of spinel is

approximately uniform at about 1% throughout the measured sequence, except in one sample that is near the clinopyroxenite vein (Figure 10).

4.2.1. Olivine

[23] Olivine compositional variations from the Trinity traverse show a number of features distinct from other sampled peridotite sequences. Figure 11 displays the Mg#, NiO and CaO of olivine as a function of position. The Mg# of olivine is nearly uniform throughout the dunite, harzburgite and lherzolite at approximately 90. The one exception is the region within the dunite associated with a thin clinopyroxenite vein where the Mg# of the olivine increases to 90.3. The Mg# of olivine increases to 90.4 within the plagioclase lherzolite. NiO in olivine is uniform throughout the dunite at 0.33% (again, except for around the clinopyroxenite vein) and increases slightly in the harzburgite (0.34%) but transitions to 0.39% starting at 2 m and remains constant throughout the remainder of the sequence. As with the modal abundance data, this transition may correspond to the change from the harzburgite to the lherzolite (Figure 10). CaO in olivine within the dunite is greater than CaO in the surrounding harzburgite. The increase of CaO in olivine within the dunite is a ubiquitous feature that

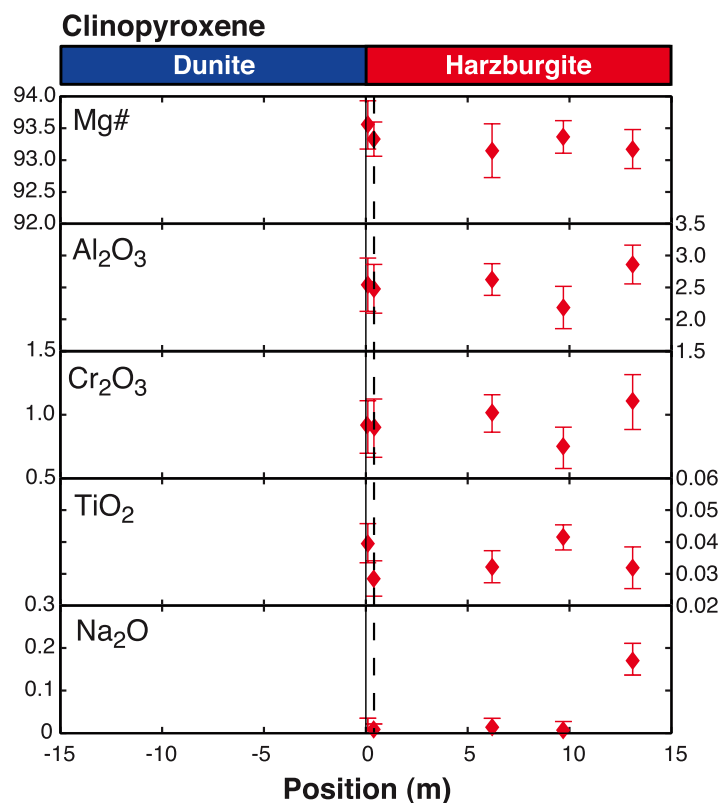


Figure 9. Composition profiles in clinopyroxene across the dunite-harzburgite sequence at the Josephine ophiolite. The red diamonds are the average of clinopyroxene analyses for each sample within the harzburgite. The error bars are 1 standard deviation about the mean of all clinopyroxene analyses for a particular sample. The distance from the dashed line to the dunite-harzburgite contact is the harzburgite boundary layer thickness.

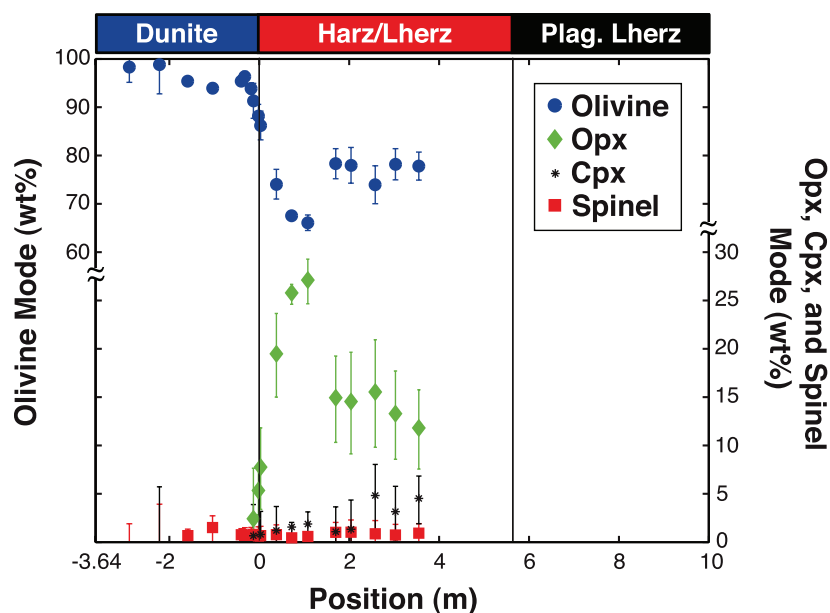


Figure 10. Modal abundance (wt%) of olivine (blue circles), opx (green diamonds), cpx (black asterisks), and spinel (red squares) in our Trinity ophiolite samples. The modal abundances were calculated from the bulk chemical data and our individual mineral analyses and are listed in Table S2b of auxiliary material Table S2.

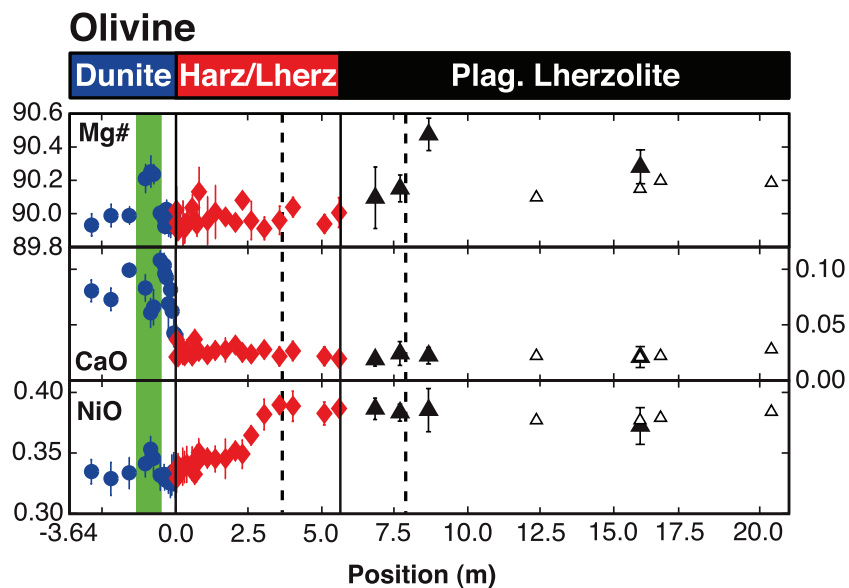


Figure 11. Composition profiles in olivine across the dunite-harzburgite-lherzolite-plagioclase lherzolite sequence at the Trinity ophiolite. The blue circles, red diamonds, and black triangles are the average of olivine analyses for each sample within the dunite, the harzburgite/lherzolite, and the plagioclase lherzolite, respectively. The error bars are 1 standard deviation about the mean of all olivine analyses for a particular sample. The distance from the dashed line in the harzburgite/lherzolite to the dunite-harzburgite contact is the harzburgite boundary layer thickness (more appropriately the NiO boundary layer thickness). The distance from the dashed line in the plagioclase lherzolite to the dunite-harzburgite contact is the plagioclase lherzolite boundary layer thickness. The green field highlights the region modified by the pyroxenite vein.

has been observed in dunite bodies in other ophiolites (Trinity [Quick, 1981a]; Iwanidake [Kubo, 2002]; Bay of Islands [Suhr et al., 2003]; Oman [Braun, 2004]; and Josephine (this study)) and is likely a result of subsolidus reequilibration (see section 5.3 for a discussion).

4.2.2. Spinel

[24] Spinel compositions from the Trinity traverse are consistent with those observed in olivine but distinct from other sampled peridotite sequences. Figure 12 displays the Mg#, MgO, FeO, Cr#, Cr₂O₃, Al₂O₃ and TiO₂ abundance in spinel as a function of position. The Mg# of the spinel within the dunite region is complicated: it increases from 38 in the dunite to 54 in the clinopyroxenite vein; it then drops abruptly to ~30 in the dunite and increases nearly linearly to ~40 at the dunite-harzburgite interface. The harzburgite and lherzolite region is relatively uniform with an Mg# of ~40. And finally, the Mg# of spinel increases within the plagioclase lherzolite relative to the harzburgite and lherzolite (Figure 12). The MgO profile in spinel has the same pattern as the Mg#, while the FeO profile is a mirror image of the Mg# and MgO profiles. The Cr# in spinel is approximately uniform throughout the dunite, harzburgite

and lherzolite, with the exception of the region around the clinopyroxenite vein where the Cr# decreases. The Cr# of spinel also decreases within the plagioclase lherzolite. Not reflected in the Cr#, the Cr₂O₃ abundance in spinel increases from the clinopyroxenite to the dunite-harzburgite contact. Al₂O₃ shows a slight increase from the clinopyroxenite vein to the dunite-harzburgite contact. The change in Cr₂O₃ and Al₂O₃ without changing the Cr# is the result of the increased FeO and Fe₂O₃ content of spinel. (Variations of calculated Fe₂O₃ in spinel are similar to those for the total FeO in spinel shown in Figure 12.) TiO₂ in spinel is approximately uniform throughout the dunite, harzburgite and lherzolite with the exception of the clinopyroxenite region and a slight concentration gradient between the clinopyroxenite vein and the dunite-harzburgite contact. Around the clinopyroxenite vein the TiO₂ content of spinel decreases. The uniform TiO₂ content in spinel continues into the plagioclase lherzolite where it transitions to about 0.70% at 12.5 m.

4.2.3. Orthopyroxene

[25] In contrast with the harzburgite and lherzolite dissolution experiments [Daines and Kohlstedt, 1994; Morgan and Liang, 2003, 2005; Beck et

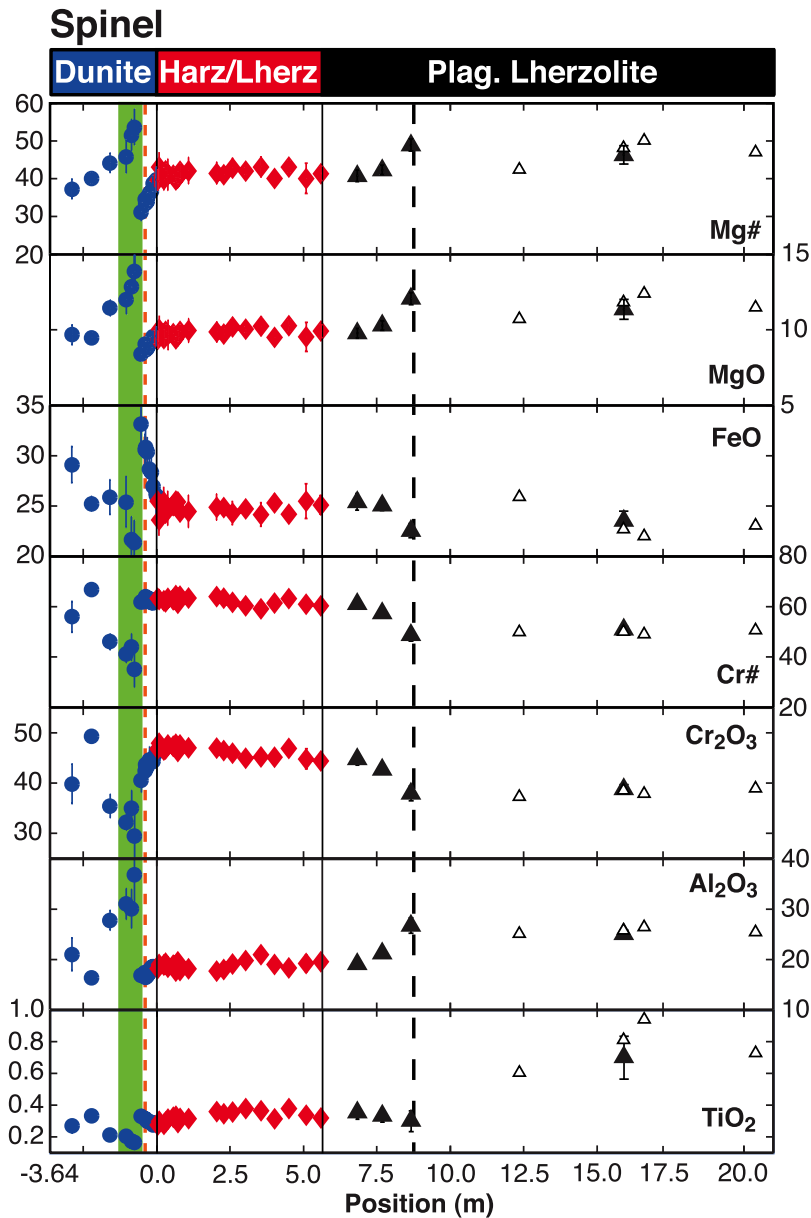


Figure 12. Composition profiles in spinel across the dunite-harzburgite-lherzolite-plagioclase lherzolite sequence at the Trinity ophiolite. The blue circles, red diamonds, and filled and open triangles are the average of spinel analyses for each sample within the dunite, the harzburgite/lherzolite, and the plagioclase lherzolite, respectively. The error bars are 1 standard deviation about the mean of all spinel analyses for a particular sample. The distance from the dunite-harzburgite contact to the orange dotted line is the dunite boundary layer thickness. The distance from the dashed line in the plagioclase lherzolite to the dunite-harzburgite contact is the plagioclase lherzolite boundary layer thickness. The green field highlights the region modified by the pyroxenite vein.

al., 2006] opx first occurs in the dunite. Within the dunite the opx abundance is low, restricted to with 0.25 m of the dunite-harzburgite contact and when it does occur it is extensively altered. The occurrence of opx in the dunite may be due to the orientation and somewhat irregular nature of the dunite-harzburgite contact (Figure 4). The contact

dips toward the dunite at 50° making it likely that some of our cores passed through the dunite into the underlying harzburgite. In addition, it is unlikely the dunite-harzburgite contact remains dipping at 50°, instead the dip of the contact may vary with depth. Figure 13 displays the opx composition as a function of position. The composition of the

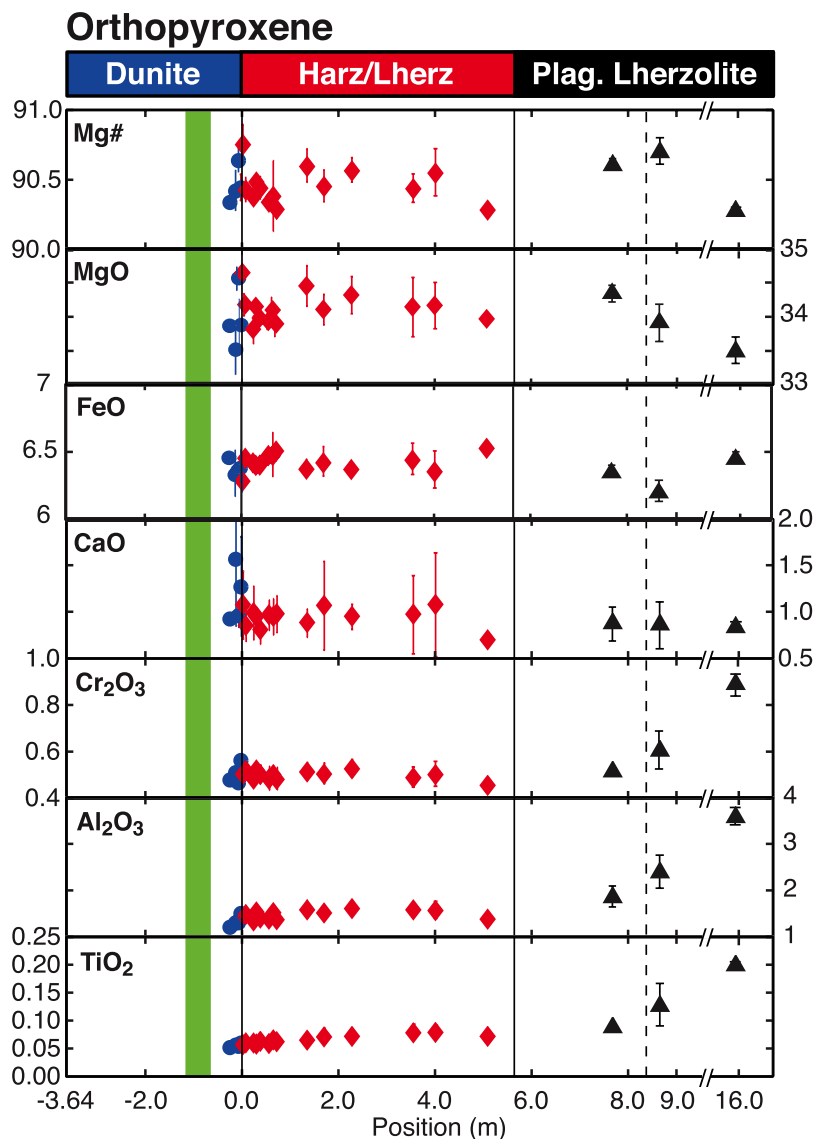


Figure 13. Composition profiles in orthopyroxene across the dunite-harzburgite-lherzolite-plagioclase lherzolite sequence at the Trinity ophiolite. The blue circles, red diamonds, and black triangles are the average of orthopyroxene analyses for each sample within the dunite, the harzburgite/lherzolite, and the plagioclase lherzolite, respectively. The error bars are 1 standard deviation about the mean of all orthopyroxene analyses for a particular sample. The green field highlights the region modified by the pyroxenite vein.

opx within the dunite and the harzburgite/lherzolite regions is approximately uniform. However, the scatter in opx compositions is large near the dunite-harzburgite contact. Within the plagioclase lherzolite the opx composition for Al_2O_3 , Cr_2O_3 and TiO_2 increases while the MgO and Mg\# decrease.

4.2.4. Clinopyroxene

[26] Clinopyroxene is found in every lithology in the Trinity traverse. The cpx abundance within the dunite is significantly lower than elsewhere in the sequence (Figure 10). The composition profiles for

cpx are shown in Figure 14. Within the dunite there are two dominant regions, the clinopyroxenite vein and the immediately surrounding dunite and the area from the clinopyroxenite vein to the dunite-harzburgite contact. The Al_2O_3 , Cr_2O_3 and TiO_2 contents of cpx in the clinopyroxenite vein are slightly higher than the surrounding dunite (Figure 14). Between the clinopyroxenite vein modified region and the dunite-harzburgite contact, the Mg\# and Al_2O_3 appear to have a gradient. Mg\# and Al_2O_3 range, respectively, from 93.1, and 2.0% next to the clinopyroxenite vein to 92.8 and 1.7%

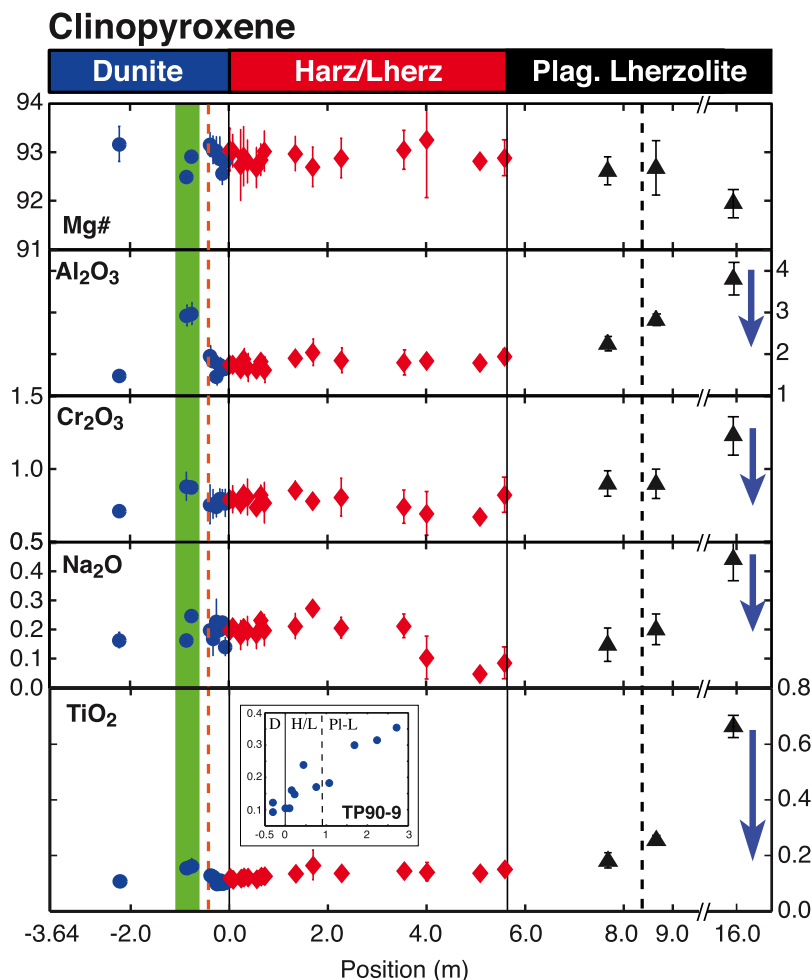


Figure 14. Composition profiles in clinopyroxene across the dunite-harzburgite-lherzolite-plagioclase lherzolite sequence at the Trinity ophiolite. The blue circles, red diamonds, and black triangles are the average of clinopyroxene analyses for each sample within the dunite, the harzburgite/lherzolite, and the plagioclase lherzolite, respectively. The error bars are 1 standard deviation about the mean of all clinopyroxene analyses for a particular sample. The blue arrows represent the core to rim variations in individual cpx (M. Lo Cascio et al., unpublished data, 2006). The inset in the TiO₂ panel is a plot of TiO₂ abundance in cpx (in wt%) versus distance (in meters) from the dunite-harzburgite contact for the transect TP90-9 (P. B. Kelemen, unpublished data, 1992). The distance from the dunite-harzburgite contact to the orange dotted line is the dunite boundary layer thickness. The distance from the dashed line to the dunite-harzburgite contact is the plagioclase lherzolite boundary layer thickness. The green field highlights the region modified by the pyroxenite vein.

at the dunite-harzburgite contact. The Mg#, Al₂O₃, Cr₂O₃ and TiO₂ contents are uniform through out the harzburgite/lherzolite region. Within the plagioclase lherzolite the compositions of Al₂O₃, Cr₂O₃, TiO₂ and Na₂O in cpx increase, similar to those observed in spinel and opx (Figures 12 and 13).

4.2.5. Rare Earth Elements

[27] To further characterize the trace element variations of the clinopyroxenite vein and the surrounding modified dunite we measured the REE

abundances of cpx in four samples. One of the samples is the clinopyroxenite vein, one is cpx in the chemically modified dunite next to the clinopyroxenite vein, and two samples are dunite outside the pyroxenite-influenced dunite. The general feature from these cpx analyses is one of light rare earth element (LREE) depletion (Figure 15a). The clinopyroxenite vein cpx has the same general REE pattern as cpx elsewhere in the dunite, but with a factor of 2 to 3 enrichment in all of the REE. In general, our measured Nd abundances in cpx in the dunite and the clinopyroxenite are in the lower end of those reported by Kelemen et al. [1992] for three

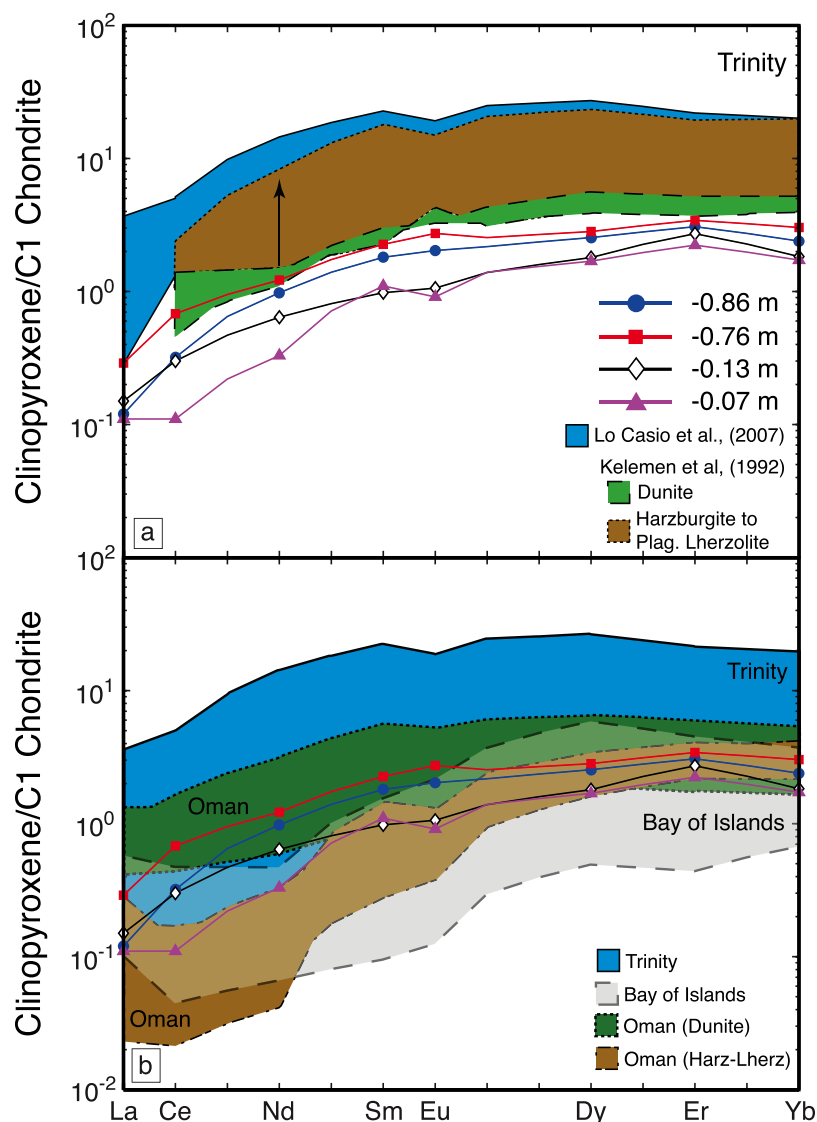


Figure 15. (a) Chondrite normalized rare earth element (REE) abundance in clinopyroxene within dunite at the Trinity ophiolite. The green field is for dunite from TP90-9 transect [Kelemen *et al.*, 1992; P. B. Kelemen, unpublished data, 1992]. The brown field is for harzburgite-lherzolite-plagioclase lherzolite from TP90-9 transect. The blue field is for plagioclase lherzolite (M. Lo Cascio *et al.*, unpublished data, 2007). (b) For comparison we also include the fields of REE data for cpx in dunite from the Oman ophiolite (green field is for the Oman dunite, and brown field is for the Oman harzburgite [Kelemen *et al.*, 1995a; Braun, 2004]) and the Bay of Islands ophiolite (gray field [Suhr *et al.*, 2003]).

different traverses (TP90-9, 9W, and 8W40) at the Trinity ophiolite (see their Figure 1).

4.2.6. Major Compositional Variations

[28] In contrast to the Josephine traverse, the chemical boundary layers are more difficult to define for the Trinity transect which contains additional lithologies (lherzolite and plagioclase lherzolite). Nevertheless, it is useful to note regions

of major compositional variations in the Trinity traverse (dashed lines in Figures 11–14). Three such regions can be easily identified in Figures 11–14: areas around the clinopyroxenite vein in the dunite; a region between the harzburgite and lherzolite where NiO abundance in olivine increases gradually; and a region in the plagioclase lherzolite where major and minor element abundance in olivine, cpx, opx, and spinel vary systematically over a distance of 1 m (between 7.5 to 8.5 m).



These major compositional variations must be accounted for in any petrological models.

5. Discussion

5.1. Comparison With Harzburgite Subtype Ophiolites

[29] Among the limited number of extensively studied harzburgite subtype ophiolites dunites and harzburgites in the Josephine ophiolite are most similar to those in the Bay of Islands ophiolite and the Oman ophiolites. With varying degrees of spatial resolution *Suhr et al.* [2003] made sampling transects across 6 dunite-harzburgite sequences. Each dunite body sampled from the Bay of Islands ophiolite is chemically distinct in major and trace elements from the other as well as any of the previously reported dunite-harzburgite sequences. Figure 1 has a schematic showing the observed variations of NiO in olivine across the dunite-harzburgite sequences at the Bay of Islands. The dunite-harzburgite sequence we measured at the Josephine ophiolite (Figures 5–9) is similar to the dunite-harzburgite sequence T1581 of *Suhr et al.* [2003] where the Mg# of olivine and Cr# of spinel all increase from harzburgite to dunite.

[30] The composition profiles for the 6 dunite-harzburgite sequences reported by *Suhr et al.* [2003] are more complicated than those we observed at the Josephine ophiolite. The composition profiles on one side of the dunite-harzburgite sequence frequently differ from those on the other side of the sequence. However, the general trends (e.g., increasing Mg# in olivine from the harzburgite to the dunite) are consistent among most of the measured elements. The exception is CaO in olivine which always has a concentration gradient restricted to the dunite. All of these are similar to our sampled dunite-harzburgite sequence from the Josephine ophiolite. In addition, *Suhr et al.* [2003] observed that the chemistry of the measured dunite-harzburgite sequences vary as a function of the dunite thickness. As the dunite width increases the mineralogy of the dunite becomes more refractory with higher Mg#s in the olivine and higher Cr#s in the spinel. However, not all elements show this consistent correlation with dunite thickness. NiO in olivine, for example, varies independently from the dunite width.

[31] *Braun* [2004] made another set of detailed composition profile measurements of dunite-harzburgite sequences in the Oman ophiolite. Similar to our

observations and those of *Suhr et al.* [2003] he found composition gradients near the dunite-harzburgite contacts. In addition, he found the chemical variations of the dunite-harzburgite sequence varied systematically with the width of the dunite. The wider dunites appear to have progressively higher TiO₂ contents in spinel and lower NiO contents in olivine.

5.2. Comparison With Lherzolite Subtype Ophiolites

[32] Earlier studies have observed compositional variations in transects across dunite and the surrounding peridotite lithologies at the Trinity ophiolite [*Quick*, 1981a; *Kelemen et al.*, 1992; *Lundstrom et al.*, 2005]. *Quick* [1981a] reported the composition variations in olivine, opx, cpx and spinel for one dunite dike (0.2 m wide) and the surrounding peridotite lithologies (0.7 m wide). A total of 5 samples were analyzed, providing little constraint on the compositional gradients. However, the samples do suggest a trend in chemical variations across the peridotite sequence. For example, the Mg#s of olivine, opx, cpx, and spinel decrease, while the TiO₂ abundance in opx, cpx, and spinel increase, from within the dunite through the harzburgite-lherzolite region and into the plagioclase lherzolite. NiO in olivine and Cr₂O₃ in opx, cpx, and spinel are uniform throughout the reported sequence. Taken together our samples and those of *Quick* [1981a] show two distinct chemical trends of dunite and surrounding peridotite lithologies in Trinity ophiolite. This compositional diversity is similar to the observations at the Bay of Islands ophiolite [*Suhr et al.*, 2003], suggesting that the composition of instantaneous melt flowing through individual dunite channel is quite variable.

[33] Figure 15a compares our measured REE abundances in cpx in the dunite (open diamonds and red triangles) and the clinopyroxenite vein (blue circles and red squares) with those from two other transects from the mantle section of the Trinity ophiolite. In general, our measured REE abundances in cpx in the dunite are lower than or in the lower range of the reported and unpublished data of REE abundance in cpx. Taken together, Figure 15a shows that REE abundance in cpx increases from the dunite to the harzburgite and the lherzolite, and finally to the plagioclase lherzolite. This is in general agreement with our measured TiO₂ abundances in spinel, opx, and cpx (Figures 12–14). Since the Nd abundance in cpx is nearly linearly correlated with the Ti abundance in cpx, both on



the grain scale [Takazawa *et al.*, 1996] and on the outcrop scale [Kelemen *et al.*, 1992, transect TP90-9], we expect that the compositional trends of REE in cpx from our Trinity transect be similar to that of TiO₂ in cpx, which is completely different from the linear trend of TiO₂ in cpx from transect TP90-9 (see inset to Figure 14). This diversity in REE abundance in cpx again suggests the heterogeneous nature of the instantaneous melt flowing through individual dunite channels.

[34] Compared to REE abundance in cpx from other ophiolites, the measured heavy rare earth elements (HREE) profiles in cpx from our 4 dunitites are similar to the ranges reported by Kelemen *et al.* [1995a] and Braun [2004] for the Oman ophiolite and by Suhr *et al.* [2003] for the Bay of Islands ophiolite (Figure 15b). The light rare earth elements (LREE) span the range between the Oman data [Kelemen *et al.*, 1995a; Braun, 2004] and the Bay of Islands data [Suhr *et al.*, 2003]. The cpx REE profiles show a great deal of overlap between all three ophiolites. The Trinity dunite is similar to dunite from the Bay of Islands [Suhr *et al.*, 2003] and Oman [Kelemen *et al.*, 1995a; Braun, 2004], with the Bay of Islands having more HREE depleted samples. The Trinity lherzolite samples are more enriched than either the Bay of Islands or Oman.

[35] A number of detailed studies have been conducted on the Horoman peridotite, Japan [e.g., Obata and Nagahara, 1987; Takahashi, 1992; Takazawa *et al.*, 1992, 1996, 2000; Saal *et al.*, 2001]. Obata and Nagahara [1987] reported bulk rock chemical variations and Mg# of olivine across a large section of the Horoman peridotite. They observed Mg# of olivine from 88 in a plagioclase lherzolite to nearly 94 within a dunite. While Obata and Nagahara [1987] see interesting variations in chemistry across several DHL-PL sequences within their traverse, the spatial resolution of their sampling is too coarse for an individual peridotite sequence. Takahashi [1992] reported individual mineral compositions across an extended peridotite section containing several sets of DHL-PL sequences. With the exception of the largest dunite and the immediately surrounding harzburgite the spatial resolution of the sampling is again too coarse to resolve detailed variations. The Mg# and NiO content of olivine and Cr# of spinel within the largest dunite reported by Takahashi [1992] are lower than in the surrounding harzburgite, while the TiO₂ of spinel in the dunite is greater than the host peridotite. The composition

gradients are mostly restricted to the dunite. Takazawa *et al.* [1996, 2000] studied the bulk rock chemical variations of the peridotite sequences from the Horoman peridotite. They found systematic variations in the bulk chemistry as a function of position in both the major and trace elements. The bulk rock Mg# decreases from the harzburgite through the lherzolite into the plagioclase lherzolite. Similarly, CaO and Al₂O₃ increase systematically from the harzburgite through the plagioclase lherzolite.

[36] Takazawa *et al.* [1992] reported REE variations in cpx as a function of position within a peridotite sequence surrounding an olivine gabbro in the same transect later studied by Takazawa *et al.* [1996, 2000]. Similar to the observations of Kelemen *et al.* [1992] at the Trinity ophiolite, they found systematic variations in REE concentrations of cpx in their sampled sequence. However, variations in the REE abundance in cpx in the sequence reported by Takazawa *et al.* [1992] are more complicated than those observed by Kelemen *et al.* [1992].

5.3. Subsolidus Reequilibration

[37] The rocks observed within ophiolites are reequilibrated at a lower temperature after the peridotite sequences have been produced. Therefore caution must be exercised when inferring magmatic history from these subsolidus samples. Subsolidus temperatures for our Josephine and Trinity samples were calculated using the two-pyroxene geothermometer of Brey and Köhler [1990] and a revised olivine-spinel geothermometer of Fabries [1979; Liu *et al.*, 1995]. For each sample we independently measured approximately 10 compositions of each mineral, olivine, spinel, opx and cpx in a thin section or a 25.4 mm diameter drill core mount. In each sample we used every spot analysis to calculate the two-pyroxene and olivine-spinel temperatures resulting in a population of temperatures (approximately 100 temperatures per sample). From this temperature population we then calculated the mean and standard deviation for the two-pyroxene and the olivine-spinel temperatures. The average two pyroxene temperature is $892 \pm 18^\circ\text{C}$ for the harzburgite from the Josephine samples. We have no temperature estimates for the dunite because no opx was found within the dunite samples in this study. The average two-pyroxene temperatures are $875 \pm 11^\circ\text{C}$ for the plagioclase lherzolite, $851 \pm 34^\circ\text{C}$ for the harzburgite/lherzolite, and $863 \pm 73^\circ\text{C}$ for the



dunite from the Trinity traverse. The average olivine-spinel temperatures from Josephine traverse are $780 \pm 22^\circ\text{C}$ for the harzburgite and $818 \pm 52^\circ\text{C}$ for the dunite, while the average olivine-spinel temperatures of the Trinity traverse are $740 \pm 7^\circ\text{C}$ for the plagioclase lherzolite, $768 \pm 15^\circ\text{C}$ for the harzburgite/lherzolite and $706 \pm 38^\circ\text{C}$ for the dunite. Interestingly, there is an apparent temperature gradient across a region of the dunite that is sandwiched between the clinopyroxenite vein and the harzburgite. The apparent temperature decrease from the dunite-harzburgite contact to the clinopyroxenite vein is correlated with a systematic decrease in spinel grain size from the harzburgite to the dunite and will be discussed elsewhere (Y. Liang et al., manuscript in preparation, 2008). Overall, the two-pyroxene temperatures are systematically higher than the olivine-spinel temperatures for both traverses. The systematic differences in the two temperatures are related to the differences in closure temperature for Fe-Mg diffusion in pyroxene and in olivine and spinel. These temperature estimates show that olivine, opx, cpx and spinel continued to reequilibrate for several hundred degrees below the magmatic temperature.

[38] The extent of subsolidus reequilibration is a function of the cooling rate as well as cation diffusivities for the minerals. This can be evaluated using the concept of closure temperature [e.g., Dodson, 1973]. Here instead of calculating the temperature at which a grain is closed to diffusion we can make estimate of the distance over which an element of interest can diffuse for a given cooling rate (s) and initial temperature (T_0). The mean square diffusion penetration distance for an element of interest, $\langle x^2 \rangle$, is given by [Lasaga, 1998]

$$\langle x^2 \rangle = 2D_0 e^{-E/RT_0} \frac{RT_0^2}{sE}, \quad (1)$$

where E and D_0 are the activation energy and preexponential factor for diffusion; s is the cooling rate; and R is the gas constant. For simplicity, we neglect grain boundary diffusion that further increases diffusive penetration distance. Figure 16 displays the root mean square diffusion penetration distance or closure distance for Ca, Ni, Cr, and Fe-Mg in olivine, Fe-Mg in spinel, Cr and Fe-Mg in opx, and Li, La and Yb in cpx as a function of cooling rate. In general, the closure distances are longer for the 2+ charged cations in olivine and spinel and considerably shorter for the 2+ and 3+ charged cations in pyroxenes. For a cooling rate of

$10^\circ\text{C}/\text{Ma}$, the closure distances are 95 m for Li in cpx, 0.5 m for Ca in olivine, 0.3 m for Fe-Mg in spinel, and 0.2 m for Ni in olivine. Further, for the 3+ cations, the closure distances are 50 and 0.5 mm for Cr in olivine and opx, respectively, and 4 and 0.7 mm for Yb and La, respectively, in cpx. The diffusion rates of Ti in cpx and opx are likely comparable to or slower than REE diffusion in the pyroxenes (D. Cherniak, personal communication, 2007). Hence subsolidus reequilibration can at most affect TiO_2 abundance in pyroxene on the mineral grain scale. Indeed, compositionally homogeneous cpx core with Ti, Cr, and REE enriched (or depleted) rim ($\sim 100\text{--}300 \mu\text{m}$ wide) have been observed in porphyroclast cpx (approximately a few millimeters in size) in lherzolite and plagioclase lherzolite from the Trinity ophiolite [Quick, 1981b; M. Lo Cascio et al., unpublished data, 2006] and the Horoman peridotite [Takazawa et al., 1996; Yoshikawa and Nakamura, 2000]. Hence concentration profiles of TiO_2 and Cr_2O_3 in opx and cpx shown in Figures 13 and 14, all measured from pyroxene cores, are most likely of magmatic origin. The strong correlations between TiO_2 and other major and minor elements in cpx and opx, respectively, suggest that magmatic trends were largely preserved in those elements as well. Possible exceptions are B and Li in cpx.

[39] Lundstrom et al. [2005] examined the B and Li abundance and Li isotopic variations in cpx from three different transects across DHL-PL sequences at the Trinity ophiolite that were originally collected by Kelemen et al. [1992]. Transect TP90-20 reported by Lundstrom et al. [2005] is the same as our Trinity transect. According to Lundstrom et al. [2005] the Li abundance in cpx increases monotonically from approximately 1 ppm in the dunite to 1.6 ppm at the lherzolite-plagioclase lherzolite boundary and to 2.5 ppm in the plagioclase lherzolite. A similar trend was also observed for B in cpx, though the analytical uncertainties are somewhat larger. The B and Li concentration profiles for cpx reported by Lundstrom et al. [2005] are distinct from any of our measured major and minor element profiles for cpx from the same sequence (compare Figure 14 and their Figure 4). Diffusion coefficients of Li and B in mantle olivine and opx have not been measured. On the basis of cation size and charge considerations and the very fast Li diffusion in cpx [Coogan et al., 2005], anorthite [Giletti and Shanahan, 1997], and Li phosphorus olivine [Morgan et al., 2004], as well as in molten silicates [Richter et al., 2003], we expect that Li diffusion in olivine and opx at least

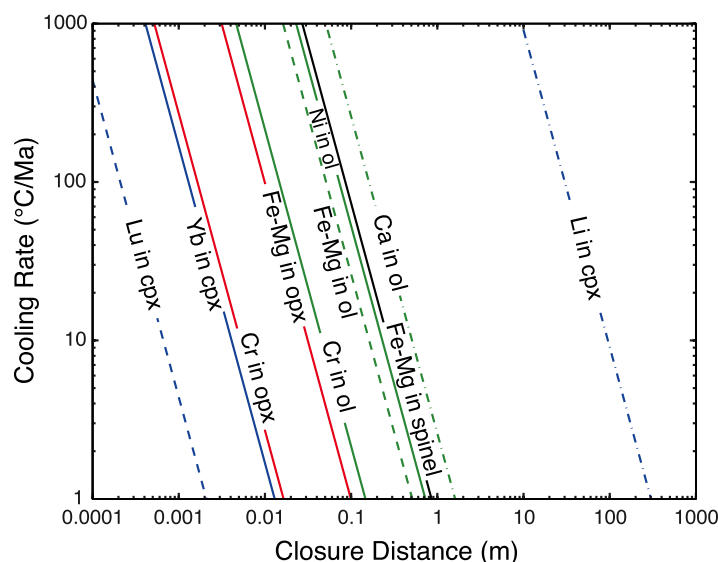
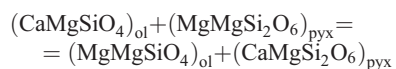


Figure 16. Calculated closure distances (m) for selected elements in selected minerals as a function of cooling rate ($^{\circ}\text{C}/\text{Ma}$) using the formulation of *Lasaga* [1998]. The diffusivities used in the calculations are as follows: for olivine, MgO-FeO [*Chakraborty*, 1997], NiO [*Ito et al.*, 1999], CaO [*Jurewicz and Watson*, 1988], and Cr_2O_3 [*Ito and Ganguly*, 2006]; for spinel, MgO [*Liermann and Ganguly*, 2002]; for opx, MgO-FeO [*Ganguly and Tazzoli*, 1992] and Cr_2O_3 [*Ganguly et al.*, 2007]; for cpx, Lu and Yb [*Van Orman et al.*, 2001], and Li [*Coogan et al.*, 2005].

one order of magnitude faster than Ca diffusion in olivine. Depending on the cooling rate, the closure distance for Li (and possibly B, too) in the dunite and harzburgite can be greater than 10 m. Hence the Li and B concentration profiles for cpx in the TP90-20 transect are likely to be significantly perturbed by subsolidus reequilibration processes.

[40] From the closure distance calculations we find that the high CaO abundances of olivine in the dunite relative to the host harzburgite and/or lherzolite in both the Josephine and Trinity ophiolites as well as other sampled dunite bodies [e.g., *Quick*, 1981a; *Takahashi*, 1992; *Kubo*, 2002; *Suhr et al.*, 2003; *Braun*, 2004] are most likely reset by subsolidus reequilibration. As the olivine/pyroxene partition coefficients for CaO decrease with the decreasing temperature [e.g., *Köhler and Brey*, 1990], CaO diffuses out of olivine and into the coexisting pyroxenes (pyx), namely,



With the exception of the rare grains of cpx, olivine is the main reservoir of CaO in the dunite. Hence the effect of subsolidus redistribution for CaO in the dunite is relatively small compared to that in the harzburgite and lherzolite. The lower abundance of CaO in olivine around the clinopyroxenite

vein in Figure 11 is clearly a result of subsolidus reequilibration. Olivine in harzburgite, lherzolite or plagioclase lherzolite that have more than 1% of cpx will reequilibrate CaO rapidly, lowering the CaO abundance in olivine.

[41] Ni is strongly partitioned into olivine during magmatic and subsolidus processes and hence its abundance in (magmatic) olivine is unlikely to be significantly altered, in spite of a moderate diffusion rate and closure distance (Figure 16). This can be further evaluated using the temperature dependent mineral-mineral trace element partition coefficients of *Witt-Eickchen and O'Neill* [2005] for spinel lherzolite. This is straightforward for fast diffusing cations such as Ni because its compositions are effectively homogeneous in coexisting mantle minerals. Hence given modal abundance and NiO content in bulk sample or olivine, we can calculate the NiO content in coexisting minerals at a prescribed temperature. The procedure is as follows: the bulk NiO content of the harzburgites, lherzolites, and the plagioclase lherzolite are first calculated using the mineral-mineral partition coefficients for NiO from *Witt-Eickchen and O'Neill* [2005] at the subsolidus temperatures determined by the two-pyroxene geothermometer of *Brey and Köhler* [1990]. The NiO content of olivine at the assumed magmatic temperature (1300°C) is then calculated from the estimated bulk NiO abundance,

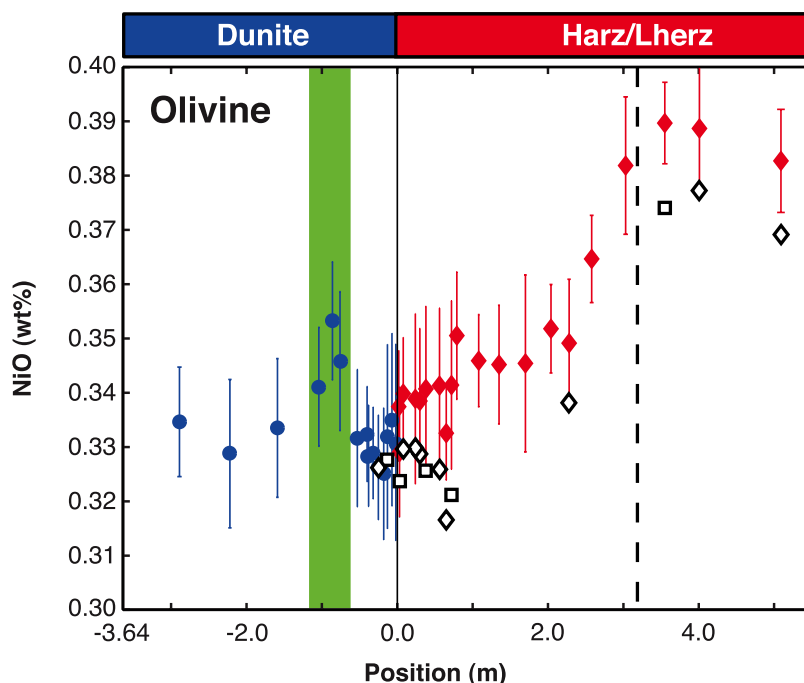


Figure 17. Variations of NiO in olivine corrected for subsolidus reequilibration for the Trinity traverse. The blue circles and red diamonds are the average of olivine analyses for each sample within the dunite, and the harzburgite/lherzolite, respectively. The open diamonds and squares are NiO compositions corrected for subsolidus equilibration (see section 5.3 for discussion).

mineral proportions, and mineral-mineral partition coefficients for NiO. The main limitations of this approach are the accuracy of the estimated modal abundance, our assumption that NiO compositions in pyroxenes are homogeneous, and the accuracy of the partition coefficients used. Figure 6 includes the NiO contents of olivine in the harzburgite corrected for the subsolidus effects for our Josephine samples (open diamonds). For our Trinity samples Figure 17 shows a smaller subsection of our sample traverse (including the dunite, harzburgite and lherzolite) illustrating the NiO contents of olivine corrected for subsolidus reequilibration (open diamonds). In general, the apparent effect of subsolidus reequilibration is to increase the NiO abundance in olivine and decrease the NiO abundance in pyroxenes. As shown in Figures 6 and 17, the relative amount is small and does not significantly modify the overall trends for NiO in olivine. The salient feature of NiO abundance in olivine from our Trinity transect is that it first decreases from the clinopyroxenite vein to the surrounding dunite and harzburgite, it then increases from the harzburgite to the lherzolite (Figure 17). As will be discussed in section 6.4, this complex compositional pattern cannot be produced by a single mag-

matic event or process. Multiple episodes of melt flow and melt-rock reaction are likely involved.

[42] Cr is strongly partitioned into spinel and Cr-diopside in spinel peridotite. The Cr-Al chemical diffusion rate in spinel is likely to be very small, on the basis of a preliminary high-pressure study of Cr-Al interdiffusion in spinel by *Suzuki et al.* [2005] which gave closure distances that are comparable to Cr in opx. The diffusion rate of Ti in spinel is likely to be slower than that of Cr-Al, on the basis of ionic size and charge considerations. Hence the complex compositional patterns of the average TiO_2 , Cr_2O_3 , and Al_2O_3 (Cr#) in spinel shown in Figure 12 are most likely of magmatic origin. Fe-Mg interdiffusion rate in spinel is relatively fast compared to those in olivine and opx [e.g., *Ganguly and Tazzoli*, 1992; *Chakraborty*, 1997; *Liermann and Ganguly*, 2002] (see also Figure 16). It is likely that MgO and FeO (hence Mg#) profiles of spinel were partially reset by subsolidus reequilibration. Nevertheless, the overall compositional trends for MgO and FeO in spinel still mimic those of 3+ and 4+ cations in spinel.

[43] In summary, concentration profiles of TiO_2 , Cr_2O_3 , and, to a lesser extent, Al_2O_3 in cpx, opx,



and spinel, as well as NiO in olivine from the dunite-harzburgite and the DHL-PL sequences are mostly likely produced by high-temperature magmatic processes. Compositional trends of FeO and MgO in the pyroxenes, olivine, and spinel were also produced by similar high-temperature processes, though the magnitudes of variation were reduced to various extent during subsolidus reequilibration. CaO abundance in olivine, as well as Li and B in cpx, across the harzburgite, lherzolite, and plagioclase lherzolite were significantly perturbed by subsolidus processes. In the next section we will examine the magmatic processes that may give rise to the compositional variations observed in the Josephine and Trinity transects.

6. Significance of Concentration Gradients

[44] With the exception of a few fast diffusing elements, the concentration gradients across the dunite-harzburgite or DHL-PL sequence were produced by magmatic processes associated with melt migration. There are a number of factors that may contribute to the development of the concentration gradients in the peridotite sequence, including but not limited to, temperature, pressure, melting rate and lithology of the host peridotite, percolating melt composition, and melt flow directions. In this study, we will focus on the last three factors.

6.1. Concentration Gradients Across the Dunite-Harzburgite Sequence

[45] A key factor controlling the development of concentration gradients across the dunite channels and associated concentration variations is the melt flow direction in the channel with respect to the orientation of the dunite-harzburgite interface. Intuitively one would expect the highest matrix dissolution rate in areas where the predominant melt flow direction in the dunite is perpendicular to the dunite-harzburgite interface, i.e., at the tips of a growing dunite channel (Figure 1). In areas far behind the propagating tips, the predominant melt flow directions in the dunite and harzburgite are probably parallel to the dunite-harzburgite interface. The rate of matrix dissolution then is limited by the rate of chemical diffusion of the major components in the interstitial melt [e.g., *Liang, 2003; Morgan and Liang, 2003, 2005*], i.e., at its minimum. Under this limiting condition, we can assume that the major and minor elements in the minerals and interstitial melts are in local chemical

equilibrium at a given position and use the following steady state conservation equation to approximate the first-order mass transfer process in the dunite and associated harzburgite,

$$V_x \frac{\partial C_f}{\partial x} + V_y \frac{\partial C_f}{\partial y} = \frac{\rho_f \phi D_f}{\rho_f \phi + \rho_s (1 - \phi) k} \frac{\partial^2 C_f}{\partial x^2}, \quad (2)$$

where C_f is the concentration in the melt in the dunite or harzburgite; V_x and V_y are components of melt velocity perpendicular (x) and parallel (y) to the dunite-harzburgite interface, respectively; k is the bulk solid-melt partition coefficient for the element of interest in the dunite or harzburgite; ρ_f and ρ_s are the melt and solid densities, respectively; ϕ is the porosity of the dunite or harzburgite; and D_f is the effective diffusion coefficient for the element of interest in the melt. The effective diffusivity is a sum of chemical diffusion and mechanic dispersion due to grain-scale melt flow in the porous rock. Since mass transfer parallel to the dunite-harzburgite interface is dominated by advection, diffusion in the y direction is neglected in equation (2). Also for simplicity, we assume that the rate of matrix melting is much smaller than the rates of diffusion and advection in the melt, though this may not be valid for a fertile peridotite.

[46] It is convenient to recast equation (2) in nondimensional form by choosing a convenient length (L) and concentration scale (C_0), namely, $C_f = C_0 C_f'$ and $(x, y) = L(x', y')$. The appropriate length scale in this case is the half width of the dunite channel. The nondimensionalized equation, after dropping the primes, is

$$\frac{\partial C_f}{\partial y} + \frac{V_x}{V_y} \frac{\partial C_f}{\partial x} = \frac{\varepsilon}{(\varepsilon + k) Pe_y} \frac{\partial^2 C_f}{\partial x^2}, \quad (3a)$$

where ε is the melt-solid mass ratio, defined as $\varepsilon = \rho_f \phi / \rho_s (1 - \phi)$; and Pe_y is a lithology specific Peclet number defined with respect to the component of melt velocity parallel to the dunite-harzburgite contact in the dunite or harzburgite, namely,

$$Pe_y = \frac{V_y L}{D_f}. \quad (3b)$$

When the effect of lateral melt flow is small compared to diffusion across the dunite-harzburgite interface ($V_x/V_y \ll 1/Pe_y$), the concentration boundary layer thickness for the dunite (δ_D) and the harzburgite (δ_H) can be estimated from the characteristic diffusion penetration distance, namely,

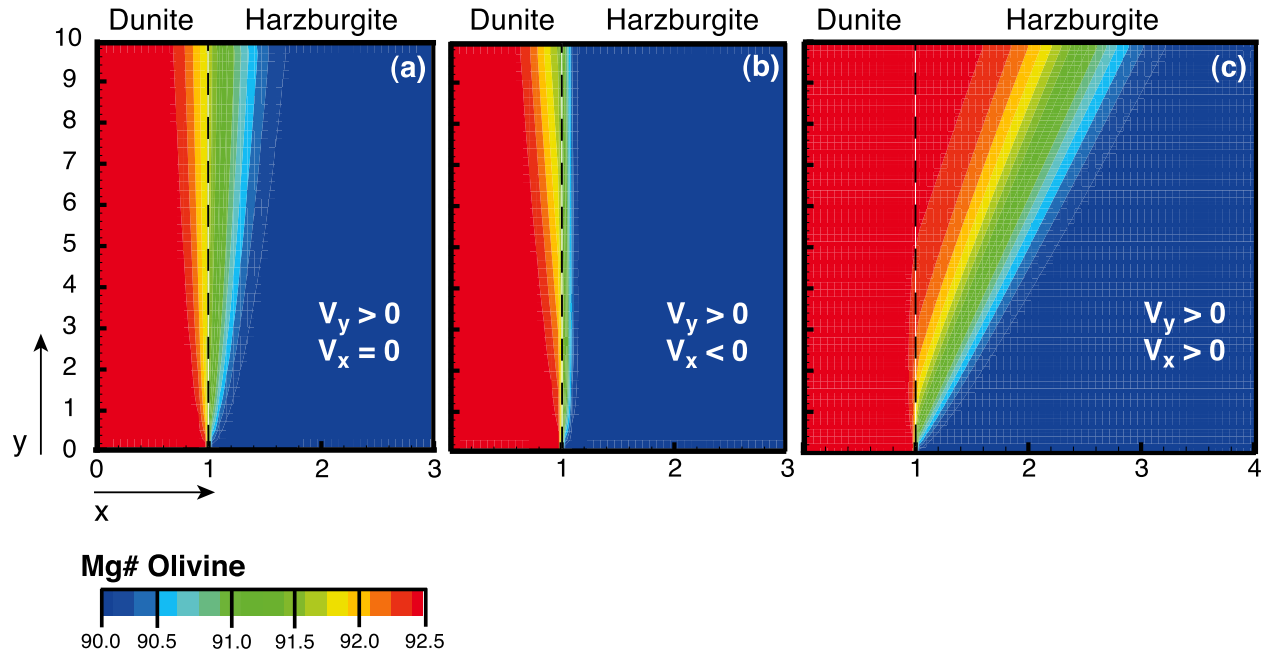


Figure 18. Numerical models illustrating variations of Mg# in olivine resulting from 2-D melt flow in a dunite channel. (a) Steady state Mg# distribution in the dunite and harzburgite when there is no melt flow across the dunite-harzburgite contact ($V_x = 0$, $V_y > 0$). (b) Steady state Mg# distribution when melt flows from the harzburgite into the dunite across the dunite-harzburgite interface ($V_x < 0$, $V_y > 0$). (c) Steady state Mg# distribution when melt flows from the dunite into the harzburgite across the dunite-harzburgite interface ($V_x > 0$, $V_y > 0$). The boundary conditions are constant melt compositions at the bottom, free flow at the top, and periodic on the two sides of the computation box. The parameters used in the numerical calculations are given by *Morgan* [2006]. Here the actual length is scaled by the half width of the dunite channel.

$$\frac{\delta_D}{L} = \sqrt{\frac{y\rho_f\phi_D D_f}{V_y^D L [\rho_f\phi_D + \rho_s(1 - \phi_D)k_D]}} \quad (4a)$$

$$\frac{\delta_H}{L} = \sqrt{\frac{y\rho_f\phi_H D_f}{V_y^H L [\rho_f\phi_H + \rho_s(1 - \phi_H)k_H]}} \quad (4b)$$

where the subscript and superscript *D* or *H* refer to properties in the dunite or harzburgite. Hence for the simple case considered here, concentration boundary layer thickness is inversely proportional to the square root of the channel-parallel melt velocity and increases linearly as a function of the square root of the channel height (*y*). The ratio of the concentration boundary thickness between the harzburgite and the dunite is independent of *y* and given by

$$\frac{\delta_H}{\delta_D} = \sqrt{\frac{\phi_H}{\phi_D} \frac{V_y^D}{V_y^H} \frac{[\rho_f\phi_D + \rho_s(1 - \phi_D)k_D]}{[\rho_f\phi_H + \rho_s(1 - \phi_H)k_H]}} \quad (5)$$

Since the channel-parallel melt velocity scales to its host permeability and the permeability of the

dunite channel is larger than that of the harzburgite matrix for melt migration in the mantle, we have $\delta_H > \delta_D$ for both the compatible and incompatible elements.

[47] Figure 18a shows an example of calculated Mg# in olivine for the case where there is no melt flow across the dunite-harzburgite interface. Details of the model calculations are given by *Morgan* [2006]. As expected from equations (4a) and (4b), the widths of the concentration boundary layers on the dunite and harzburgite side of the interface increase with the square root of height. Further, the ratios of the harzburgite to dunite concentration boundary layer thicknesses are practically independent of column height (compare to equation (5)), resulting in an asymmetric concentration profile across the dunite-harzburgite interface. Figure 19 compares our calculated relative concentration boundary layer thickness between the dunite and harzburgite for the case of no lateral melt flow (squares) with those observed from the Bay of Islands ophiolite [*Suhr et al.*, 2003], Horoman peridotite [*Takahashi*, 1992], Iwanidake peridotite [*Kubo*, 2002], and our Josephine measurements. Models run without horizontal melt

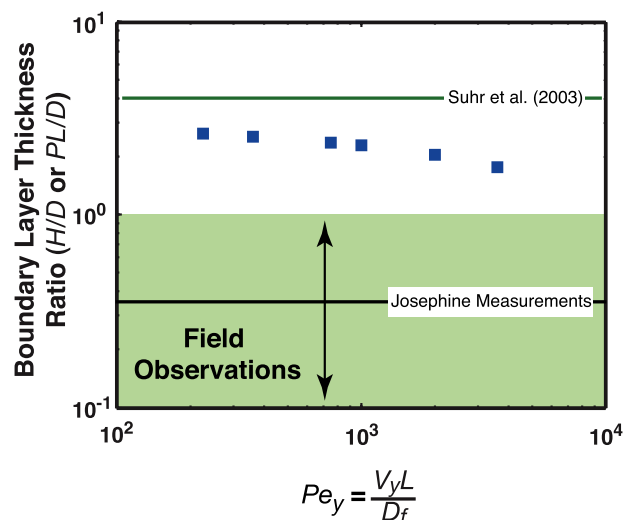


Figure 19. Plot of harzburgite/dunite (H/D) or plagioclase ilherzolite/dunite (PL/D) boundary layer thickness ratios as a function of the vertical fluid velocity for numerical models where there is no melt flow across the dunite-harzburgite contact. The blue squares are our numerical data, the green field corresponds to ophiolite field observations, including our Josephine measurement, and the line at $H/D = 4$ is from *Suhr et al.* [2003].

flow do not match the field observations. The model results have harzburgite concentration boundary layer thicknesses 2 to 3 times greater than the dunite concentration boundary layer thicknesses. This conclusion likely remains valid when diffusive dissolution of the harzburgite matrix is included [Morgan and Liang, 2003, Figure 10]. To date, there is only one published dunite-harzburgite transect from the Bay of Islands ophiolite [Suhr et al., 2003] that shows the concentration boundary layer thickness on the harzburgite side is about 4 times larger than that on the dunite side (Figure 19). If this was produced by diffusion alone, equation (5) suggests that the porosity in the harzburgite is at least 4 times smaller than the porosity in the dunite. Most field observations, however, have harzburgite boundary layer thicknesses equal to or less than the dunite boundary layer thicknesses. Lateral melt flow, in addition to diffusive mass transfer across the dunite-harzburgite interface, must be involved.

[48] When there is lateral melt flow across the dunite-harzburgite interface, the concentration boundary layer thickness on either side of the lithological contact will be changed, depending on the direction of melt flow [e.g., Bickle and McKenzie, 1987]. When melt flows from the harzburgite into the dunite, the concentration boundary layer thickness for the harzburgite will be com-

pressed, whereas the concentration boundary layer thickness on the dunite side of the interface will be stretched. The opposite is true when the melt flow direction is reversed.

[49] Figures 18b shows an example of the calculated Mg# of olivine in the dunite and the harzburgite when there is a component of melt flowing from the harzburgite into the dunite. The asymmetric composition gradients are restricted to the vicinity of the dunite-harzburgite contact with the majority of compositional variations occurring within the dunite. The degree of asymmetry in this case is determined by the relative strength of lateral advection to the strength of diffusion in the porous dunite and the harzburgite, as well as the channel-parallel Peclet number (compare to equation (3a)). If the velocity of the melt entering the dunite from the harzburgite is sufficiently large, the concentration boundary layer thickness on the dunite side of the interface will be greater than that on the harzburgite side, in contrast to the case of no lateral melt flow (compare to Figures 18a and 18b). This will result in little or no modification of the host harzburgite by the reacting basalt. The melt composition in the dunite can be significantly affected by this lateral flow. Such lateral melt flow or melt suction has been shown to play an important role in the fractionation of trace element in the melt during concurrent melting and melt migration in the mantle [e.g., Iwamori, 1994; Lundstrom, 2000; Jull et al., 2002; Liang, 2008]. Figure 20 shows the results of our numerical simulations for a number of horizontal flow velocities at a constant vertical flow rate (squares). With increasing lateral melt flow rate, the dunite composition boundary layer thicknesses progressively increases, whereas the harzburgite composition boundary layer decreases. The dunite composition boundary layer is only thicker than the harzburgite boundary layer when there is melt flow entering the dunite from the harzburgite and the volume of incoming melt is on the order of melt flow in the dunite. In general, these model results are consistent with most of the reported field observations, including our measurements from the Josephine ophiolite.

[50] When the pressure of the melt in the dunite is greater than that in the harzburgite, melt flows from the dunite into the harzburgite. This situation can be found in places near or around the front of a propagating dunite channel or in regions where there is a significant amount of compaction in the dunite. Figures 18c shows an example of the calculated Mg# of olivine in the dunite and the harzburgite for a case

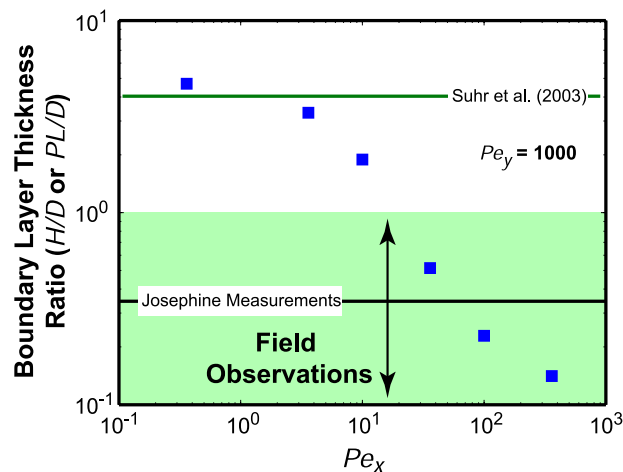


Figure 20. Plot of harzburgite/dunite (H/D) or plagioclase lherzolite/dunite (PL/D) boundary layer thickness ratios as a function of the horizontal fluid velocity for models with melt flow from the dunite across the dunite-harzburgite contact. Pe_y is the vertical Peclet number defined as $(V_y L/D_f)$. Pe_x is the horizontal Peclet number with the same definition as Pe_y except we use the maximum horizontal fluid velocity $(V_x L/D_f)$. The blue squares are our numerical data, the green field corresponds to ophiolite field observations, including our Josephine measurement, and the line at $H/D = 4$ is from Suhr et al. [2003].

when there is a component of melt flowing from the dunite into the harzburgite. Compared to the case of no lateral melt flow (Figure 18a), regions of significant compositional variations are now shifted to the harzburgite side of the interface. If the velocity of melt flowing out of the dunite is sufficiently high, the dunite boundary layer thickness may approach zero. The consequences of melt flowing from the dunite into the harzburgite are (1) an enhanced rate of harzburgite dissolution and (2) the modification of the harzburgite composition; the latter may have important implications for compositions of the melts derived from the dunite and the harzburgite. These model results appear to be consistent with our measurements from the Trinity ophiolite.

6.2. Concentration Gradients Across the DHL-PL Sequence at the Trinity Ophiolite

[51] The lithology and compositional patterns associated with our Trinity transect are more complicated than the Josephine transect (compare Figures 6–9 and 11–14) and those observed in our lherzolite diffusive dissolution experiments [Morgan and Liang, 2005]. It is likely that the major and minor element compositional profiles

recorded in the cores of olivine, opx, cpx, and spinel from the Trinity transect (Figures 11–14 and 17) were produced by complicated magmatic processes, involving multiple episodes of melt flow. Multiple episodes of melt flow in the mantle, each with possibly distinct elemental and isotopic characteristics, have already been documented in olivine-hosted melt inclusions. One possible scenario that is capable of producing the observed concentration profiles is outlined below. Following Quick [1981b], we assume that plagioclase in the plagioclase-bearing lherzolite was formed by basalt impregnation when the partially molten lherzolite cooled below the plagioclase liquidus. This is similar to the interpretation for the origin of plagioclase-bearing abyssal peridotite [e.g., Dick, 1989; Elthon, 1992; Niu and Hékinian, 1997].

[52] Dissolution of a partially molten lherzolite by a percolating, pyroxene-undersaturated basalt resulted in reactive infiltration instability [e.g., Aharonov et al., 1995, 1997; Spiegelman et al., 2001] and formation of the dunite-harzburgite-lherzolite sequence [e.g., Quick, 1981a; Morgan and Liang, 2005]. The major and minor element concentration gradients recorded in the four minerals in the now plagioclase lherzolite (regions between 7.5 and 9 m in Figures 11–14), as well as the nearly uniform concentration profiles for most of the oxides (except NiO in olivine, Figure 17) in the harzburgite and lherzolite, could be produced by reaction between the peridotites and a melt percolating from the dunite into the harzburgite and lherzolite. Since NiO is highly compatible and diffuses relatively fast in olivine, its infiltration front is lagged behind other major elements and incompatible minor and trace elements, as a result of mantle chromatography [e.g., McKenzie, 1984; Navon and Stolper, 1987; Bodinier et al., 1990]. This is also consistent with the irregular, wavy dunite-harzburgite lithological contact in the field (Figure 4). The morphology of a planar dunite-harzburgite interface can be destabilized by the flow of melt from the dunite into the harzburgite. It would be practically impossible to produce the observed concentration profiles, such as TiO_2 and Cr_2O_3 in the pyroxenes and spinel, by reaction and percolation of a melt from the lherzolite into the dunite. It is possible that the concentration profiles of Li and B in cpx reported by Lundstrom et al. [2005] for the same Trinity transect had been originally similar to those of Na_2O and TiO_2 in cpx shown in Figure 14 and were later relaxed to the present nearly linear profiles by subsolidus reequilibration. Nevertheless, the nearly linear concentration profiles for the slow



diffusing cations Nd and Ti in cpx from another Trinity traverse reported by *Kelemen et al.* [1992] (TP90-9; also see the inset to Figure 14) are consistent with simple diffusive dissolution with or without small amount of melt flowing from the lherzolite into the dunite.

[53] And finally, the nearly linear concentration profiles around the clinopyroxenite vein are likely associated with the late emplacement of the vein in the dunite. The host peridotites were likely partially molten at the time. This is supported by (1) the relatively wide concentration boundary layers on either side of the vein that cannot be produced by diffusion in the solid alone; (2) a systematic decrease in spinel grain size from the clinopyroxenite vein to the dunite-harzburgite interface that were likely produced by spinel partial dissolution during melt-peridotite interaction (Y. Liang et al., manuscript in preparation, 2008); and (3) the nonlinear geometry of the vein (Figure 4). The asymmetric concentration patterns on either side of the vein were probably controlled by the surrounding lithology: dunite on the east (left in Figures 11–14) and dunite-harzburgite on west (right) side of the vein. The origin of the clinopyroxenite vein itself is still not well constrained at this stage, owing to limited sampling and chemical data. At least two possible scenarios should be considered: (1) flow and precipitation of melt derived from the deeper part of the mantle and (2) flow and precipitation of melt from the lherzolite and harzburgite into the dunite during late stage cooling, crystallization, compaction and closure of the dunite channel system. Scenario 2 may be consistent with the local increase in opx modal abundance in the harzburgite and the presence of a few opx grains on the dunite side of the dunite-harzburgite interface. Clearly more work is needed to further constrain the various interpretations outline in this section.

7. Summary and Conclusions

[54] Motivated by our laboratory studies of harzburgite and lherzolite reactive dissolution in basaltic magmas [*Morgan and Liang, 2003, 2005*] we have conducted detailed 1-D chemical mapping across a dunite-harzburgite sequence at the Josephine ophiolite and a DHL-PL sequence at the Trinity ophiolite. Results from our chemical analysis are then compared with those from other ophiolites and simple 2-D numerical simulations. The main conclusions of this study are summarized as follows:

[55] 1. At the Josephine ophiolite composition profiles were observed within olivine and spinel as a function of position across the dunite and the host harzburgite. The first-order features of the profiles are similar to those observed at the Bay of Islands ophiolite [*Suhr et al., 2003*] and Oman ophiolite [*Braun, 2004*] with asymmetric composition gradients resulting concentration boundary layers in the dunite wider than those in the harzburgite.

[56] 2. At the Trinity ophiolite concentration profiles were observed within olivine, spinel, opx, and cpx as a function of position across the DHL-PL sequence. The first-order features of the Trinity profiles are distinct from any of the composition profiles previously observed in ophiolites. These include asymmetric composition gradients resulting in harzburgite and plagioclase lherzolite boundary layers wider than the dunite boundary layer. The presence of a later clinopyroxenite vein has a significant effect on narrow region within the dunite.

[57] 3. Our measured concentration profiles and REE abundance in cpx from the Trinity ophiolite are different from the previously reported ones from the Trinity ophiolite [*Quick, 1981a; Kelemen et al., 1992; Lundstrom et al., 2005*]. This adds additional evidence that concentration profiles in dunite and the surrounding peridotite lithologies are highly variable even among differing peridotite sequences within the same ophiolite. An important implication of this observation is that the composition of instantaneous melt flowing through individual dunite channel is quite variable, suggesting with the heterogeneous nature of the mantle source region.

[58] 4. Detailed analyses of closure distance suggest that compositional variation trends for a majority of major and minor elements in olivine, cpx, opx, and spinel reported in this study were magmatic in origin. Subsolvus reequilibration may reduce the range or magnitude of variations for the 2+ cations such as Fe and Mg in olivine and spinel and significantly redistribute the Ca, Li, and possibly B abundance in coexisting minerals.

[59] 5. In comparison to the concentration profiles produced by simple diffusive dissolution, concentration profiles from the Josephine and Trinity ophiolites are much more complicated. This increased complexity is undoubtedly related to the additional processes such as deformation and multiple episodes of melt flow that occur within the Earth's mantle.



[60] 6. Using simple 2-D numerical simulations we explored the effect of melt flow and flow direction on the composition profiles across the dunite-harzburgite contact. In addition to melt flow parallel to the dunite-harzburgite contact, a component of melt flow across the dunite-harzburgite contact will have a profound effect on the resulting composition profiles. In cases where melt flows from the harzburgite into the dunite, the chemical boundary layers that develop will be asymmetric, with relatively wide dunite boundary layers and narrow harzburgite boundary layers. In cases where melt flows from the dunite into the harzburgite, the composition profile will be asymmetric with most of the compositional variations occurring within the surrounding harzburgite, lherzolite or plagioclase lherzolite and little or no chemical boundary layer within the dunite.

[61] 7. Comparison of our measured composition profiles and those from simple numerical calculations lead to the conclusion that the composition profiles observed within our samples from the Josephine ophiolite results from melt flow from the harzburgite into the dunite.

[62] 8. The composition profiles observed within the Trinity traverse result from lateral melt flow from the dunite into the surrounding harzburgite, lherzolite and plagioclase lherzolite. Melt flow from the dunite causes the DHL-PL sequence to grow and results in the wider plagioclase lherzolite boundary layers.

[63] 9. As we have demonstrated through simple analyses and 2-D numerical calculations in section 7, concentration gradients or boundary layer thickness around a dunite-harzburgite contact vary along the dunite channel and are likely to provide valuable information on the rate and directions of melt migration in the mantle. We hope the simple 1-D field study reported here will stimulate additional field works that map the chemical structure of a dunite channel system in two and three dimensions in the future.

Acknowledgments

[64] We wish to thank Alyssa Beck, Paul Hess, Marc Parmentier, Marshall Sundberg, and Mac Rutherford for comments and suggestions on earlier versions of this paper. We also wish to thank Henry Dick, Eiichi Takazawa, and the senior Editor Vincent Salters for their helpful and constructive reviews. The bulk of the samples used in this study were collected through an ophiolite field course offered by Peter Kelemen and Greg Hirth at the Woods Hole Oceanographic Institution. We wish to thank Karen Hanghøj for assistance in

the field and with sample preparation, Mauro Lo Cascio, Matt Jackson, Marshall Sundberg, Jessica Warren, and Rhea Workman for assistance collecting and cataloging the samples, Jesse Kass for additional microprobe work on the Trinity samples (4 open triangles in Figures 11 and 12), and Mike Braun for sharing his unpublished data from Oman Ophiolite. This work was supported in part by a course development fund from the Woods Hole Oceanographic Institution, Brown University Fund for Geology Field Experiences made possible by alumni contributions, and NSF grants EAR-0208141 and EAR-0510606 to Y.L.

References

- Aharonov, E., J. Whitehead, P. B. Kelemen, and M. Spiegelman (1995), Channeling instability of upwelling melt in the mantle, *J. Geophys. Res.*, *100*, 20,433–20,450, doi:10.1029/95JB01307.
- Aharonov, E., M. Spiegelman, and P. Kelemen (1997), Three-dimensional flow and reaction in porous media: Implications for the Earth's mantle and sedimentary basins, *J. Geophys. Res.*, *102*, 14,821–14,834, doi:10.1029/97JB00996.
- Beck, A. R., Z. T. Morgan, Y. Liang, and P. C. Hess (2006), Dunite channels as viable pathways for mare basalt transport in the deep lunar mantle, *Geophys. Res. Lett.*, *33*, L01202, doi:10.1029/2005GL024008.
- Bickle, M. J., and D. McKenzie (1987), The transport of heat and matter by fluids during metamorphism, *Contrib. Mineral. Petrol.*, *95*, 384–392, doi:10.1007/BF00371852.
- Bodinier, J. L., G. Vasseur, J. Vernieres, C. Dupuy, and J. Fabries (1990), Mechanisms of mantle metasomatism: Geochemical evidence from the Lherz orogenic peridotite, *J. Petrol.*, *31*, 597–628.
- Boudier, F., and A. Nicolas (1985), Harzburgite and lherzolite subtypes in ophiolitic and oceanic environments, *Earth Planet. Sci. Lett.*, *76*, 84–92, doi:10.1016/0012-821X(85)90150-5.
- Braun, M. G. (2004), Petrologic and microstructural constraints on focused melt transport in dunitess and the rheology of the shallow mantle, Ph.D. thesis, Mass. Inst. of Technol., Cambridge.
- Brey, G. P., and T. Köhler (1990), Geothermobarometry in 4-phase lherzolites: 2. New thermobarometers, and practical assessment of existing thermobarometers, *J. Petrol.*, *31*, 1353–1378.
- Carter, B. A., and J. E. Quick (1987), The ultramafic rocks at Eunice bluff, Trinity peridotite, Klamath mountains, California, in *Cordilleran Section of the Geological Society of America, Centen. Field Guide*, vol. 1, pp. 283–288, Geol. Soc. of Am., Boulder, Colo.
- Chakraborty, S. (1997), Rates and mechanisms of Fe-Mg interdiffusion in olivine at 980°C–1300°C, *J. Geophys. Res.*, *102*, 12,317–12,331, doi:10.1029/97JB00208.
- Coogan, L. A., S. A. Kasemann, and S. Chakraborty (2005), Rates of hydrothermal cooling of new oceanic upper crust derived from lithium-geospeedometry, *Earth Planet. Sci. Lett.*, *240*, 415–424, doi:10.1016/j.epsl.2005.09.020.
- Daines, M. J., and D. L. Kohlstedt (1994), The transition from porous to channelized flow due to melt/rock reaction during melt migration, *Geophys. Res. Lett.*, *21*, 145–148, doi:10.1029/93GL03052.
- Dick, H. J. B. (1977a), Evidence of partial melting in the Josephine peridotite, in *Magma Genesis*, edited by H. J. B. Dick, *Bull. Oreg. Dep. Geol. Miner. Ind.*, *96*, 59–62.



- Dick, H. J. B. (1977b), Partial melting in the Josephine peridotite I, The effect on mineral composition and its consequence for geobarometry and geothermometry, *Am. J. Sci.*, **277**, 801–832.
- Dick, H. J. B. (1989), Abyssal peridotites, very slow spreading ridges and ocean ridge magmatism, *Geol. Soc. Spec. Publ.*, **42**, 71–105.
- Dodson, M. H. (1973), Closure temperature in cooling geochronological and petrological systems *Contrib. Mineral. Petrol.*, **40**, 259–274, doi:10.1007/BF00373790.
- Elthon, D. (1992), Chemical trends in abyssal peridotites: Refertilization of depleted oceanic mantle, *J. Geophys. Res.*, **97**, 9015–9025, doi:10.1029/92JB00723.
- Fabries, J. (1979), Spinel-olivine geothermometry in peridotites from ultramafic complexes, *Contrib. Mineral. Petrol.*, **69**, 329–336, doi:10.1007/BF00372258.
- Ganguly, J., and V. Tazzoli (1992), Fe²⁺-Mg interdiffusion in orthopyroxene: Constraints from cation ordering and structural data and implications for cooling rates of meteorites (abstract), *Lunar Planet. Sci.*, **XXIV**, 517–518.
- Ganguly, J., M. Ito, and X. Zhang (2007), Cr diffusion in orthopyroxene: Experimental determination, ⁵³Mn-⁵³Cr thermochronology, and planetary applications, *Geochim. Cosmochim. Acta*, **71**, 3915–3925, doi:10.1016/j.gca.2007.05.023.
- Giletti, B. J., and T. M. Shanahan (1997), Alkali diffusion in plagioclase feldspar, *Chem. Geol.*, **139**, 3–20, doi:10.1016/S0009-2541(97)00026-0.
- Gruau, G., J. Bernard-Griffiths, C. Lécuyer, O. Henin, J. Macé, and M. Cannat (1995), Extreme Nd isotopic variation in the Trinity Ophiolite Complex and the role of melt/rock reactions in the oceanic lithosphere, *Contrib. Mineral. Petrol.*, **121**, 337–350, doi:10.1007/s004100050100.
- Harper, G. D. (1980), The Josephine ophiolite: Remains of a Late Jurassic marginal basin in northwestern California, *Geology*, **8**, 333–337, doi:10.1130/0091-7613(1980)8<333:TJOOAL>2.0.CO;2.
- Harper, G. D. (1984), The Josephine ophiolite, northwestern California, *Geol. Soc. Am. Bull.*, **95**, 1009–1026, doi:10.1130/0016-7606(1984)95<1009:TJONC>2.0.CO;2.
- Himmelberg, G. R., and R. A. Loney (1973), Petrology of the Vulcan peak alpine-type peridotite, southwestern Oregon, *Geol. Soc. Am. Bull.*, **84**, 1585–1600, doi:10.1130/0016-7606(1973)84<1585:POTVPA>2.0.CO;2.
- Ito, M., and J. Ganguly (2006), Diffusion kinetics of Cr in olivine and ⁵³Mn-⁵³Cr thermochronology of early solar system objects, *Geochim. Cosmochim. Acta*, **70**, 799–809, doi:10.1016/j.gca.2005.09.020.
- Ito, M., H. Yurimoto, M. Morioka, and H. Nagasawa (1999), Co²⁺ and Ni²⁺ diffusion in olivine determined by secondary ion mass spectrometry, *Phys. Chem. Miner.*, **26**, 425–431, doi:10.1007/s002690050204.
- Iwamori, H. (1994), ²³⁸U-²³⁰Th-²²⁶Ra and ²³⁵U-²³¹Pa disequilibria produced by mantle melting and porous and channel flows, *Earth Planet. Sci. Lett.*, **125**, 1–16, doi:10.1016/0012-821X(94)90203-8.
- Jacobsen, S. B., J. E. Quick, and G. J. Wasserburg (1984), A Nd and Sr isotopic study of the Trinity peridotite: Implications for mantle evolution, *Earth Planet. Sci. Lett.*, **68**, 361–378, doi:10.1016/0012-821X(84)90122-5.
- Jull, M., P. B. Kelemen, and K. Sims (2002), Consequences of diffuse and channeled porous melt migration on Uranium series disequilibria, *Geochim. Cosmochim. Acta*, **66**, 4133–4148, doi:10.1016/S0016-7037(02)00984-5.
- Jurewicz, A. J. G., and E. B. Watson (1988), Cations in olivine, Part 2: Diffusion in olivine xenocrysts, with applications to petrology and mineral physics, *Contrib. Mineral. Petrol.*, **99**, 186–201, doi:10.1007/BF00371460.
- Kelemen, P. B., and H. J. B. Dick (1995), Focused melt flow and localized deformation in the upper mantle: Juxtaposition of replacive dunite and ductile shear zones in the Josephine peridotite, SW Oregon, *J. Geophys. Res.*, **100**, 423–438, doi:10.1029/94JB02063.
- Kelemen, P. B., H. J. B. Dick, and J. E. Quick (1992), Formation of harzburgite by pervasive melt/rock reaction in the upper mantle, *Nature*, **358**, 635–641, doi:10.1038/358635a0.
- Kelemen, P. B., N. Shimizu, and V. J. M. Salters (1995a), Extraction of mid-ocean-ridge basalt from the upwelling mantle by focused flow of melt in dunite channels, *Nature*, **375**, 747–753, doi:10.1038/375747a0.
- Kelemen, P. B., J. A. Whitehead, E. Aharonov, and K. A. Jordahl (1995b), Experiments on flow focusing in soluble porous media, with applications to melt extraction from the mantle, *J. Geophys. Res.*, **100**, 475–496, doi:10.1029/94JB02544.
- Kelemen, P. B., G. Hirth, N. Shimizu, M. Spiegelman, and H. J. B. Dick (1997), A review of melt migration processes in the adiabatically upwelling mantle beneath oceanic spreading ridges, *Philos. Trans. R. Soc. London, Ser. A*, **355**, 283–318, doi:10.1098/rsta.1997.0010.
- Köhler, T. P., and G. P. Brey (1990), Calcium exchange between olivine and clinopyroxene calibrated as a geothermobarometer for natural peridotites from 2 to 60 kb with applications, *Geochim. Cosmochim. Acta*, **54**, 2375–2388, doi:10.1016/0016-7037(90)90226-B.
- Kubo, K. (2002), Dunite formation processes in highly depleted peridotite: Case study of the Iwanadake peridotite, Hokkaido, Japan, *J. Petrol.*, **43**, 423–448, doi:10.1093/petrology/43.3.423.
- Lasaga, A. C. (1998), *Kinetic Theory in the Earth Sciences*, Princeton Univ. Press, Princeton, N. J.
- Liang, Y. (2003), Kinetics of crystal-melt reaction in partially molten silicates: 1. Grain scale processes, *Geochem. Geophys. Geosyst.*, **4**(5), 1045, doi:10.1029/2002GC000375.
- Liang, Y. (2008), Simple models for concurrent melting and melt migration in an upwelling heterogeneous mantle column: Analytical solutions, *Geochim. Cosmochim. Acta*, doi:10.1016/j.gca.2008.05.050, in press.
- Liermann, H.-P., and J. Ganguly (2002), Diffusion kinetics of Fe²⁺ and Mg in aluminous spinel: Experimental determination and applications, *Geochim. Cosmochim. Acta*, **66**, 2903–2913, doi:10.1016/S0016-7037(02)00875-X.
- Liu, J., J. Kornprobst, D. Vielzeuf, and J. Fabries (1995), An improved experimental calibration of the olivine-spinel geothermometer, *Chin. J. Geochem.*, **14**, 68–77, doi:10.1007/BF02840385.
- Loney, R. A., and G. R. Himmelberg (1976), Structure of the Vulcan Peak alpine-type peridotite, southwestern Oregon, *Geol. Soc. Am. Bull.*, **87**, 259–274, doi:10.1130/0016-7606(1976)87<259:SOTVPA>2.0.CO;2.
- Lundstrom, C. C. (2000), Models of U-series disequilibrium generation in MORB: The effect of two scales of melt porosity, *Phys. Earth Planet. Inter.*, **121**, 189–204, doi:10.1016/S0031-9201(00)00168-0.
- Lundstrom, C. C., M. Chaussidon, A. T. Hsui, P. Kelemen, and M. Zimmerman (2005), Observations of Li isotopic variations in the Trinity ophiolite: Evidence for isotopic fractionation by diffusion during mantle melting, *Geochim. Cosmochim. Acta*, **69**, 735–751, doi:10.1016/j.gca.2004.08.004.



- McKenzie, D. (1984), The generation and compaction of partially molten rock, *J. Petrol.*, *25*, 713–765.
- Morgan, D., A. Van der Ven, and G. Ceder (2004), Li conductivity in Li_xMPO_4 (M = Mn, Fe, Co, Ni) olivine materials, *Electrochem. Solid State Lett.*, *7*, A30–A32, doi:10.1149/1.1633511.
- Morgan, Z. T. (2006), Kinetics of melt-rock reaction with applications to melt transport in the Earth's mantle and the lunar crust, Ph.D. thesis, Brown Univ., Providence, R. I.
- Morgan, Z. T., and Y. Liang (2003), An experimental and numerical study of the kinetics of harzburgite reactive dissolution with applications to dunite dike formation, *Earth Planet. Sci. Lett.*, *214*, 59–74, doi:10.1016/S0012-821X(03)00375-3.
- Morgan, Z. T., and Y. Liang (2005), An experimental study of the kinetics of ilherzolite reactive dissolution with applications to melt channel formation, *Contrib. Mineral. Petrol.*, *150*, 369–385, doi:10.1007/s00410-005-0033-8.
- Navon, O., and E. Stolper (1987), Geochemical consequences of melt percolation: The upper mantle as a chromatographic column, *J. Geol.*, *95*, 285–307.
- Niu, Y., and R. Hékinian (1997), Basaltic liquids and harzburgitic residues in the Garrett Transform: A case study at fast-spreading ridges, *Earth Planet. Sci. Lett.*, *146*, 243–258, doi:10.1016/S0012-821X(96)00218-X.
- Obata, M., and N. Nagahara (1987), Layering of alpine-type peridotite and the segregation of partial melt in the upper mantle, *J. Geophys. Res.*, *92*, 3467–3474, doi:10.1029/JB092iB05p03467.
- Quick, J. E. (1981a), The origin and significance of large, tabular dunite bodies in the Trinity peridotite, northern California, *Contrib. Mineral. Petrol.*, *78*, 413–422, doi:10.1007/BF00375203.
- Quick, J. E. (1981b), Petrology and petrogenesis of the Trinity peridotite, an upper mantle diapir in the eastern Klamath Mountains, northern California, *J. Geophys. Res.*, *86*, 11,837–11,863, doi:10.1029/JB086iB12p11837.
- Richter, F. M., A. M. Davis, D. J. DePaolo, and E. B. Watson (2003), Isotope fractionation by chemical diffusion between molten basalt and rhyolite, *Geochim. Cosmochim. Acta*, *67*, 3905–3923, doi:10.1016/S0016-7037(03)00174-1.
- Saal, A. E., E. Takazawa, F. A. Frey, N. Shimizu, and S. R. Hart (2001), Re-Os isotopes in the Horoman peridotite: Evidence for refertilization?, *J. Petrol.*, *42*, 25–37, doi:10.1093/ptrology/42.1.25.
- Saleeby, J. B., G. D. Harper, A. W. Snoke, and W. D. Sharp (1982), Time relations and structural-stratigraphic patterns in ophiolite accretion, west central Klamath mountains, California, *J. Geophys. Res.*, *87*, 3831–3848, doi:10.1029/JB087iB05p03831.
- Shimizu, N., and S. R. Hart (1982), Applications of the ion microprobe to geochemistry and cosmochemistry, *Annu. Rev. Earth Planet. Sci.*, *10*, 483–526, doi:10.1146/annurev.ea.10.050182.002411.
- Spiegelman, M., P. B. Kelemen, and E. Aharonov (2001), Causes and consequences of flow organization during melt transport: The reactive infiltration instability in compactible media, *J. Geophys. Res.*, *106*, 2061–2077, doi:10.1029/2000JB900240.
- Suhr, G., E. Hellebrand, J. E. Snow, H. A. Seck, and A. W. Hofmann (2003), Significance of large, refractory dunite bodies in the upper mantle of the Bay of Islands Ophiolite, *Geochim. Geophys. Geosyst.*, *4*(3), 8605, doi:10.1029/2001GC000277.
- Suzuki, A., A. Yasuda, and K. Ozawa (2005), Cr-Al diffusion in chromite spinel at high pressure, *Eos Trans. AGU*, *86*(52), Fall Meet. Suppl., Abstract V13A-0521.
- Takahashi, N. (1992), Evidence for melt segregation towards fractures in the Horoman mantle peridotite complex, *Nature*, *359*, 52–55, doi:10.1038/359052a0.
- Takazawa, E., F. A. Frey, N. Shimizu, M. Obata, and J. L. Bodinier (1992), Geochemical evidence for melt migration and reaction in the upper mantle, *Nature*, *359*, 55–58, doi:10.1038/359055a0.
- Takazawa, E., F. A. Frey, N. Shimizu, and M. Obata (1996), Evolution of the Horoman peridotite (Hokkaido, Japan): Implications from pyroxene compositions, *Chem. Geol.*, *134*, 3–26, doi:10.1016/S0009-2541(96)00083-6.
- Takazawa, E., F. A. Frey, N. Shimizu, and M. Obata (2000), Whole rock compositional variations in an upper mantle peridotite (Horoman, Hokkaido, Japan): Are they consistent with a partial melting process?, *Geochim. Cosmochim. Acta*, *64*, 695–716, doi:10.1016/S0016-7037(99)00346-4.
- Van Orman, J. A., T. L. Grove, and N. Shimizu (2001), Rare earth element diffusion in diopside: Influence of temperature, pressure, and ionic radius, and an elastic model for diffusion in silicates, *Contrib. Mineral. Petrol.*, *141*, 687–703.
- Wallin, E. T., and R. V. Metcalf (1998), Supra-subduction zone ophiolite formed in an extensional forearc: Trinity terrane, Klamath mountains, California, *J. Geol.*, *106*, 591–608.
- Witt-Eickschen, G., and H. S. C. O'Neill (2005), The effect of temperature on the equilibrium distribution of trace elements between clinopyroxene, orthopyroxene, olivine and spinel in upper mantle peridotite, *Chem. Geol.*, *221*, 65–101, doi:10.1016/j.chemgeo.2005.04.005.
- Yoshikawa, M., and E. Nakamura (2000), Geochemical evolution of the Horoman peridotite complex: Implications for melt extraction, metasomatism, and compositional layering in the mantle, *J. Geophys. Res.*, *105*, 2879–2901, doi:10.1029/1999JB900344.
- Zhou, M.-F., P. T. Robinson, J. Malpas, S. J. Edwards, and L. Qi (2005), REE and PGE geochemical constraints on the formation of dunites in the Luobusa ophiolite, southern Tibet, *J. Petrol.*, *46*, 615–639, doi:10.1093/ptrology/egh091.